



Trastuzumab deruxtecan in metastatic breast cancer with variable HER2 expression: the phase 2 DAISY trial

Fernanda Mosele, Elise Deluche, Amelie Lusque, Loïc Le Bescond, Thomas Filleron, Yoann Pradat, Agnes Ducoulombier, Barbara Pistilli, Thomas Bachelot, Frederic Viret, et al.

► To cite this version:

Fernanda Mosele, Elise Deluche, Amelie Lusque, Loïc Le Bescond, Thomas Filleron, et al.. Trastuzumab deruxtecan in metastatic breast cancer with variable HER2 expression: the phase 2 DAISY trial. *Nature Medicine*, 2023, 29 (8), pp.2110 - 2120. <10.1038/s41591-023-02478-2>. <hal-04187928>

HAL Id: hal-04187928

<https://hal.science/hal-04187928v1>

Submitted on 25 Aug 2023

HAL is a multi-disciplinary open access archive for the deposit and dissemination of scientific research documents, whether they are published or not. The documents may come from teaching and research institutions in France or abroad, or from public or private research centers.

L'archive ouverte pluridisciplinaire **HAL**, est destinée au dépôt et à la diffusion de documents scientifiques de niveau recherche, publiés ou non, émanant des établissements d'enseignement et de recherche français ou étrangers, des laboratoires publics ou privés.




Distributed under a Creative Commons CC BY 4.0 - Attribution - International License

Trastuzumab deruxtecan in metastatic breast cancer with variable HER2 expression: the phase 2 DAISY trial

Received: 20 September 2022

Accepted: 28 June 2023

Published online: 24 July 2023

 Check for updates

Fernanda Mosele^{1,2}, Elise Deluche^{3,20}, Amelie Lusque^{4,20},
Loïc Le Bescond^{1,5,6,20}, Thomas Filleron⁴, Yoann Pradat⁷,
Agnes Ducoulombier⁸, Barbara Pistilli², Thomas Bachelot⁹, Frederic Viret¹⁰,
Christelle Levy¹¹, Nicolas Signolle¹², Alexia Alfaro¹³, Diep T. N. Tran¹,
Ingrid Judith Garberis¹⁴, Hugues Talbot^{5,6}, Stergios Christodoulidis⁷,
Maria Vakalopoulou^{6,7}, Nathalie Droin¹², Aurelie Stourm¹², Maki Kobayashi¹⁵,
Tomoya Kakegawa¹⁵, Ludovic Lacroix^{12,14}, Patrick Saulnier^{12,14}, Bastien Job¹²,
Marc Deloger¹², Marta Jimenez¹⁶, Celine Mahier¹⁶, Vianney Baris¹⁷,
Pierre Laplante¹⁷, Patricia Kannouche¹⁷, Virginie Marty¹²,
Magali Lacroix-Triki^{14,20}, Veronique Diéras^{18,20} & Fabrice André^{1,2,19,20} ✉

The mechanisms of action of and resistance to trastuzumab deruxtecan (T-DXd), an anti-HER2–drug conjugate for breast cancer treatment, remain unclear. The phase 2 DAISY trial evaluated the efficacy of T-DXd in patients with HER2-overexpressing ($n = 72$, cohort 1), HER2-low ($n = 74$, cohort 2) and HER2 non-expressing ($n = 40$, cohort 3) metastatic breast cancer. In the full analysis set population ($n = 177$), the confirmed objective response rate (primary endpoint) was 70.6% (95% confidence interval (CI) 58.3–81) in cohort 1, 37.5% (95% CI 26.4–49.7) in cohort 2 and 29.7% (95% CI 15.9–47) in cohort 3. The primary endpoint was met in cohorts 1 and 2. Secondary endpoints included safety. No new safety signals were observed. During treatment, HER2-expressing tumors ($n = 4$) presented strong T-DXd staining. Conversely, HER2 immunohistochemistry 0 samples ($n = 3$) presented no or very few T-DXd staining (Pearson correlation coefficient $r = 0.75$, $P = 0.053$). Among patients with HER2 immunohistochemistry 0 metastatic breast cancer, 5 of 14 (35.7%, 95% CI 12.8–64.9) with *ERBB2* expression below the median presented a confirmed objective response as compared to 3 of 10 (30%, 95% CI 6.7–65.2) with *ERBB2* expression above the median. Although HER2 expression is a determinant of T-DXd efficacy, our study suggests that additional mechanisms may also be involved. (ClinicalTrials.gov identifier [NCT04132960](https://clinicaltrials.gov/ct2/show/study/NCT04132960).)

Breast cancer is the fifth leading cause of cancer mortality¹. Despite advances in precision medicine and improvements in treatment, the 5-year survival rate of patients with metastases is only 30%^{2–4}. Breast cancer includes three main subtypes: hormone receptor-positive;

HER2-overexpressing; and triple-negative breast cancer (TNBC)⁵. The standard first-line treatment for patients with HER2-overexpressing metastatic breast cancer (mBC) is anti-HER2 in combination with taxanes⁶. Antibody–drug conjugates (ADCs) are drugs that deliver

A full list of affiliations appears at the end of the paper. ✉ e-mail: fabrice.andre@gustaveroussy.fr

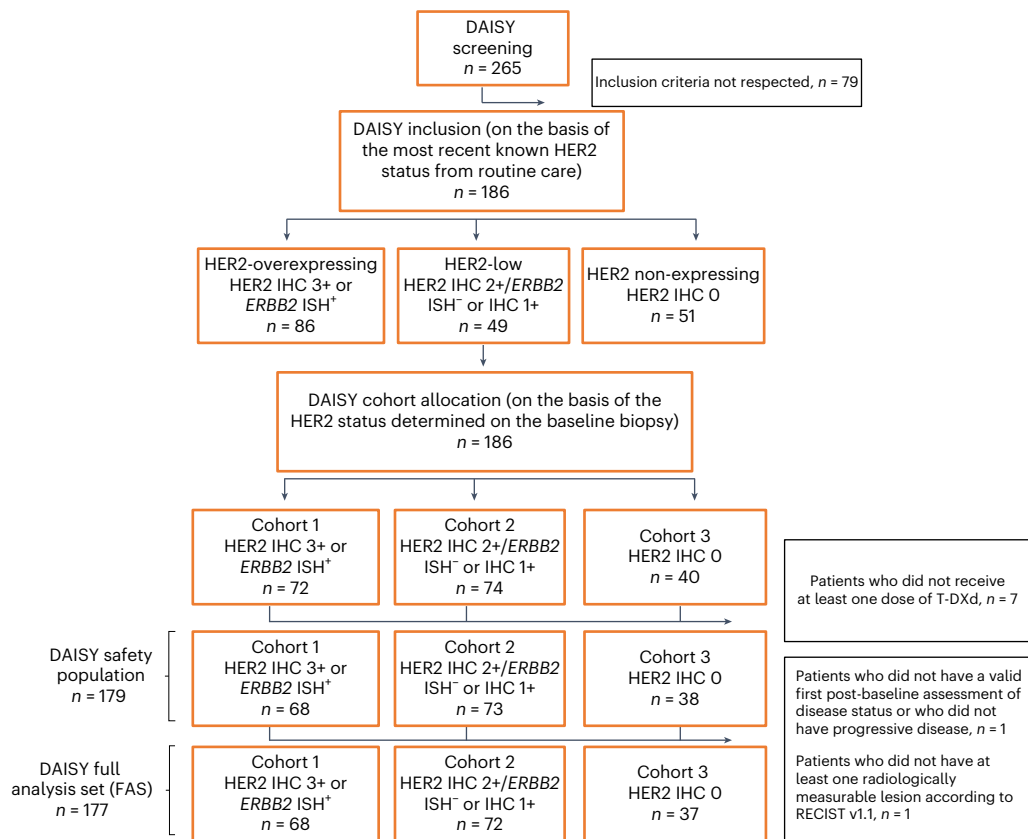


Fig. 1 | CONSORT diagram. IHC⁺, IHC-positive; IHC⁻, IHC-negative.

a cytotoxic payload to cells that express a specific target protein. Trastuzumab deruxtecan (T-DXd, DS-8201a) is a third-generation ADC composed of a humanized monoclonal anti-HER2 (trastuzumab), a cleavable tetra peptide linker and a topoisomerase 1 (TOP1) inhibitor (DXd) as the cytotoxic payload. T-DXd is characterized by a high drug-to-antibody ratio (DAR) of 8:1 (ref. 7). Trastuzumab emtansine (T-DM1) is a second-generation ADC that consists of trastuzumab conjugated by a non-cleavable linker to the cytotoxic payload emtansine (DM1), a microtubule inhibitory agent. The DAR is 3.5:1 (ref. 8). The standard second-line treatment for HER2-overexpressing mBC was T-DM1 until the approval of T-DXd in 2022 (refs. 9,10). The approval was based on DB-03, a phase 3 clinical trial, in which T-DXd improved progression-free survival (PFS) as compared to T-DM1 in patients with HER2-overexpressing mBC (hazard ratio (HR): 0.28, $P < 0.001$)¹⁰. In addition, in DB-01, a phase 2 single-arm study, T-DXd demonstrated high anti-tumor activity in patients with HER2-overexpressing mBC who had previously received T-DM1 (ref. 11). These results were confirmed in the phase 3 randomized trial DB-02 (ref. 12). Patients with HER2-low mBC are treated according to expression of hormone receptors¹³. In this group of patients, T-DXd was recently shown to be superior to systemic chemotherapy in the second line of therapy and beyond, improving PFS (HR: 0.50, $P < 0.001$) and overall survival (OS; HR: 0.64, $P = 0.001$) in patients with HER2-low mBC as compared to chemotherapy¹⁴.

Although T-DXd provides some clinical benefit in patients with HER2-overexpressing and HER2-low mBC, most of them will ultimately experience disease progression and die. Although the overall structure of T-DXd is well defined, several questions remain regarding its mechanisms of action and resistance. These include the impact of HER2 expression and its spatial distribution on drug efficacy; the distribution of T-DXd in the tumor; the potential impact on the tumor microenvironment; and the molecular mechanisms of resistance. Understanding these mechanisms of action and resistance could lead to improved

treatment selection for patients and the potential development of more effective combinatorial treatment strategies. To address these questions, we designed DAISY, a phase 2 trial that evaluated T-DXd efficacy in patients with mBC according to HER2 expression levels and explored treatment response and resistance through biomarker analyses of tumor samples at different timepoints.

Results

Study design

Patients with mBC were eligible if they had received at least one line of chemotherapy in the metastatic setting and had at least one non-bone metastatic site easily accessible to biopsy. Patients with HER2-overexpressing mBC had to be pretreated with taxanes and to be resistant to trastuzumab and TDM-1. Patients with HER2-low or HER2 immunohistochemistry (IHC) 0 tumor had to be pretreated with anthracyclines and taxanes. Patients with tumors expressing hormone receptors (estrogen and/or progesterone) had to be resistant to endocrine therapy and CDK4/6 inhibitors. Tumor biopsy was mandatory at baseline and at resistance and was optional during treatment. Additional details about patient selection and the trial design are provided in the Methods section.

In total, 186 patients were enrolled into the DAISY trial between 4 November 2019 and 3 March 2021 (Extended Data Fig. 1 and Fig. 1). Patients were assigned to a specific cohort according to HER2 status defined based on the baseline biopsy performed at study entry (Methods). Seventy-two patients with HER2-overexpressing mBC defined as IHC 3+ or ERBB2 in situ hybridization (ISH)-positive were assigned to cohort 1; 74 patients with HER2-low mBC defined as IHC 2+/ERBB2 ISH-negative or IHC 1+ were assigned to cohort 2; and 40 patients with non-expressing mBC defined as HER2 IHC 0 were assigned to cohort 3. Some patients presented a change in the HER2 status of the biopsy at baseline as compared to routine care and were,

Table 1 | Patient characteristics in the safety population

	Overall population <i>n</i> =179	Cohort 1 <i>n</i> =68	Cohort 2 <i>n</i> =73	Cohort 3 <i>n</i> =38	<i>P</i> value
Age at inclusion (years)					0.68
Median (range)	55 (24–82)	56 (30–81)	55 (24–82)	54 (36–74)	
Sex					NA
Male	1 (0.6%)	0	1 (1.4%)	0	
Female	178 (99.4%)	68 (100%)	72 (98.6%)	38 (100%)	
ECOG performance status at inclusion					0.011
ECOG 0	77 (43.0%)	21 (30.9%)	33 (45.2%)	23 (60.5%)	
ECOG 1	102 (57.0%)	47 (69.1%)	40 (54.8%)	15 (39.5%)	
Hormone receptor status of primary tumor					0.13
Hormone receptor-negative	51 (28.5%)	24 (35.3%)	15 (20.5%)	12 (31.6%)	
Hormone receptor-positive	128 (71.5%)	44 (64.7%)	58 (79.5%)	26 (68.4%)	
Most recent known HER2 status from routine care before DAISY inclusion (on primary or metastases)					NA
IHC 0	49 (27.4%)	0	21 (28.8%)	28 (73.7%)	
IHC 1+	25 (14%)	1 (1.5%)	19 (26%)	5 (13.2%)	
IHC 2+/ERBB2 ISH-negative	23 (12.8%)	0	19 (26%)	4 (10.5%)	
IHC 2+/ERBB2 ISH-positive	21 (11.7%)	11 (16.2%)	9 (12.3%)	1 (2.6%)	
IHC 3+	60 (33.5%)	56 (82.3%)	4 (5.5%)	0	
IHC 1+/ERBB2 ISH-positive	1 (0.6%)	0	1 (1.4%)	0	
HER2 status determined on the baseline biopsy for DAISY cohort allocation (on primary or metastases)					NA
IHC 0	38 (21.2%)	0	0	38 (100%)	
IHC 1+	41 (22.9%)	0	41 (56.2%)	0	
IHC 2+/ERBB2 ISH-negative	32 (17.9%)	0	32 (43.8%)	0	
IHC 2+/ERBB2 ISH-positive	17 (9.5%)	17 (25%)	0	0	
IHC 3+	50 (27.9%)	50 (73.5%)	0	0	
IHC 1+/ERBB2 ISH-positive	1 (0.6%)	1 (1.5%)	0	0	
Interval from initial diagnosis to metastatic disease					0.17
0–3 months	49 (27.4%)	24 (35.3%)	17 (23.3%)	8 (21.1%)	
>3 months	130 (72.6%)	44 (64.7%)	56 (76.7%)	30 (78.9%)	
Interval from metastatic disease to inclusion					0.62
0–24 months	45 (25.1%)	13 (19.1%)	20 (27.4%)	12 (31.6%)	
24–60 months	74 (41.3%)	29 (42.6%)	30 (41.1%)	15 (39.5%)	
>60 months	60 (33.5%)	26 (38.2%)	23 (31.5%)	11 (28.9%)	
Number of metastatic sites at inclusion					0.96
<3	63 (35.2%)	24 (35.3%)	25 (34.2%)	14 (36.8%)	
≥3	116 (64.8%)	44 (64.7%)	48 (65.8%)	24 (63.2%)	
Sites of metastasis at inclusion					
Liver					<0.001
No	76 (42.5%)	45 (66.2%)	20 (27.4%)	11 (28.9%)	
Yes	103 (57.5%)	23 (33.8%)	53 (72.6%)	27 (71.1%)	
Lung					0.56
No	103 (57.5%)	36 (52.9%)	43 (58.9%)	24 (63.2%)	
Yes	76 (42.5%)	32 (47.1%)	30 (41.1%)	14 (36.8%)	
Previous chemotherapy in any setting					NA
Yes	179 (100%)	68 (100%)	73 (100%)	38 (100%)	
Neoadjuvant					0.88
No	119 (66.5%)	46 (67.6%)	49 (67.1%)	24 (63.2%)	
Yes	60 (33.5%)	22 (32.4%)	24 (32.9%)	14 (36.8%)	
Adjuvant					0.058

Table 1 (continued) | Patient characteristics in the safety population

	Overall population <i>n</i> =179	Cohort 1 <i>n</i> =68	Cohort 2 <i>n</i> =73	Cohort 3 <i>n</i> =38	<i>P</i> value
No	105 (58.7%)	47 (69.1%)	36 (49.3%)	22 (57.9%)	
Yes	74 (41.3%)	21 (30.9%)	37 (50.7%)	16 (42.1%)	
Metastatic					0.83
No	4 (2.2%)	2 (2.9%)	1 (1.4%)	1 (2.6%)	
Yes	175 (97.8%)	66 (97.1%)	72 (98.6%)	37 (97.4%)	
Previous hormonotherapy if hormone receptor-positive on primary tumor in any setting (<i>n</i> =128)					0.002
No	9 (7.0%)	8 (18.2%)	1 (1.7%)	0	
Yes	119 (93.0%)	36 (81.8%)	57 (98.3%)	26 (100%)	
Neoadjuvant					0.59
No	115 (97.5%)	36 (100%)	54 (96.4%)	25 (96.2%)	
Yes	3 (2.5%)	0	2 (3.6%)	1 (3.8%)	
Missing	1	0	1	0	
Adjuvant					
No	42 (35.6%)	17 (47.2%)	16 (28.6%)	9 (34.6%)	
Yes	76 (64.4%)	19 (52.8%)	40 (71.4%)	17 (65.4%)	
Missing	1	0	1	0	
Metastatic					
No	13 (11.0%)	6 (16.7%)	6 (10.7%)	1 (3.8%)	
Yes	105 (89.0%)	30 (83.3%)	50 (89.3%)	25 (96.2%)	
Missing	1	0	1	0	
Previous targeted therapy in any setting					
No	17 (9.5%)	1 (1.5%)	7 (9.6%)	9 (23.7%)	
Yes	162 (90.5%)	67 (98.5%)	66 (90.4%)	29 (76.3%)	
Neoadjuvant					0.001
No	141 (87.6%)	51 (76.1%)	61 (93.8%)	29 (100%)	
Yes	20 (12.4%)	16 (23.9%)	4 (6.2%)	0	
Missing	1	0	1	0	
Adjuvant					
No	119 (73.9%)	33 (49.3%)	59 (90.8%)	27 (93.1%)	
Yes	42 (26.1%)	34 (50.7%)	6 (9.2%)	2 (6.9%)	
Missing	1	0	1	0	
Metastatic					
No	3 (1.9%)	2 (3.0%)	0	1 (3.4%)	
Yes	158 (98.1%)	65 (97.0%)	65 (100%)	28 (96.6%)	
Missing	1	0	1	0	
Previous lines of treatment in metastatic setting					
<5 lines	84 (46.9%)	32 (47.1%)	35 (47.9%)	17 (44.7%)	
≥5 lines	95 (53.1%)	36 (52.9%)	38 (52.1%)	21 (55.3%)	

Comparison among cohorts was performed using chi-square test or Fisher's exact test for qualitative variables and Kruskal–Wallis test for continuous variables. NA, not applicable.

therefore, reassigned to different cohorts (Extended Data Fig. 2). Of the 86 patients with HER2-overexpressing mBC, 14 were enrolled after baseline biopsy into cohort 2 (HER2-low, *n* = 74) and one into cohort 3 (HER2 IHC 0, *n* = 40). Of the patients with HER2-low tumors (*n* = 49), one was enrolled into cohort 1 (HER2-overexpressing, *n* = 72) and nine into cohort 3 (HER2 IHC 0, *n* = 40). Twenty-one of the fifty-one patients with HER2-non expressing mBC were enrolled into cohort 2 (HER2-low, *n* = 74). Patients received T-DXd 5.4 mg kg⁻¹ every 3 weeks until progressive disease or unacceptable toxicity. Baseline patient characteristics in the safety population (*n* = 179) are reported in Table 1. A total of 44 patients (64.7%) in cohort 1, 58 (79.5%) in cohort 2, and

26 (68.4%) in cohort 3 had hormone receptor-positive primary breast cancer (*P* = 0.13 among the three cohorts). Most patients (53.1%) were heavily pretreated with ≥5 lines of previous therapies in the metastatic setting. A total of 53 patients (72.6%) in cohort 2 and 27 (71.1%) in cohort 3 presented liver metastases at inclusion as compared to 23 (33.8%) in cohort 1 (*P* < 0.0001). There were 21 patients (30.9%) in cohort 1, 33 (45.2%) in cohort 2 and 23 (60.5%) in cohort 3 that presented an Eastern Cooperative Oncology Group (ECOG) performance status of 0 (*P* = 0.011). Prior therapy exposures were consistent with the molecular profile of breast cancer. Patient characteristics were balanced among the cohorts, except for site of metastases and performance status.

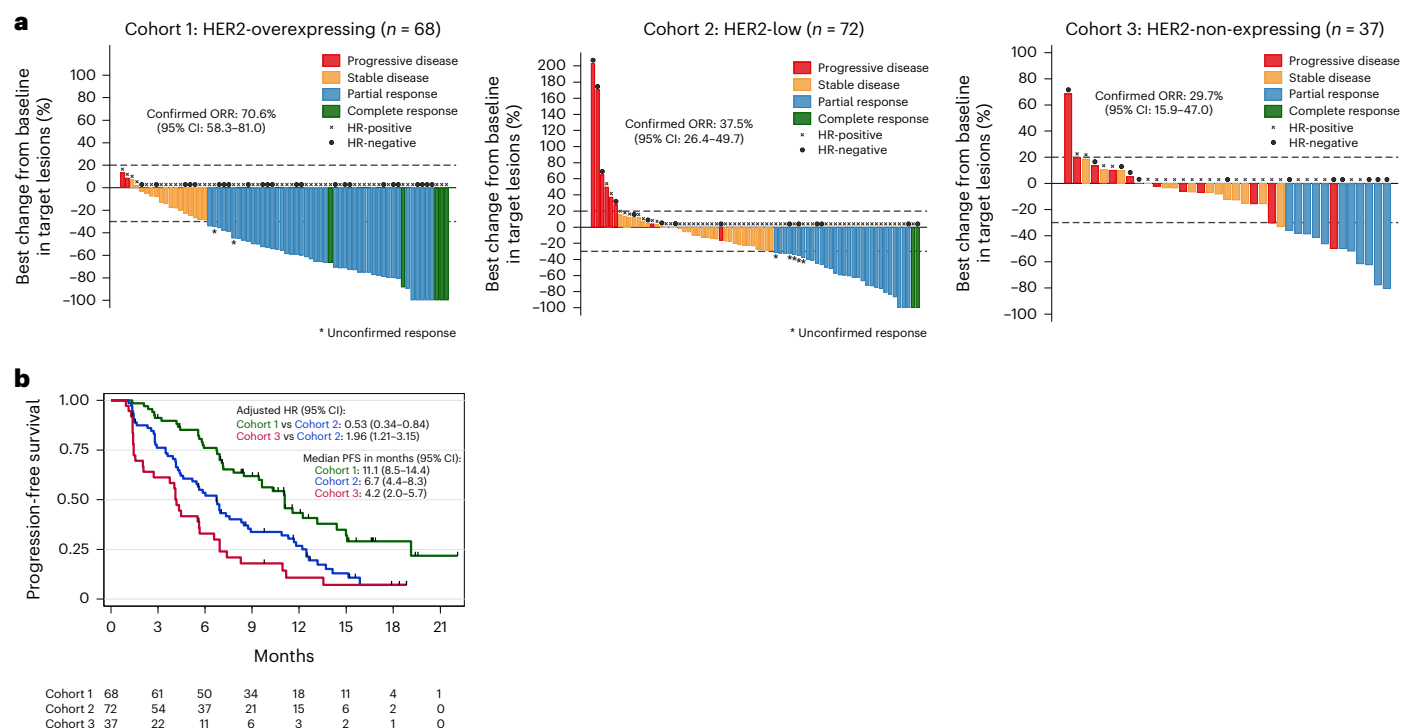


Fig. 2 | Efficacy of T-DXd per cohort. a, Waterfall plot of the best change from baseline in target lesions according to the best objective response per cohort in the FAS population ($n = 177$). The confirmed ORR with T-DXd was 70.6% ($n = 68$, 95% CI 58.3–81) in cohort 1, 37.5% ($n = 72$, 95% CI 26.4–49.7) in cohort 2 and 29.7% ($n = 37$, 95% CI 15.9–47) in cohort 3. The likelihood of confirmed objective response was higher in cohort 1 as compared to cohort 2 (adjusted OR: 3.96, 95% CI 1.78–8.77, $P = 0.001$) and not significantly different between cohort 3 and cohort 2 (adjusted OR: 0.63, 95% CI 0.25–1.54, $P = 0.30$). The adjusted OR and P value were derived from a multivariable logistic model taking as reference cohort 2 and adjusted for hormone receptor status, interval from initial diagnosis to metastatic disease, number and type of metastatic site,

ECOG performance status and interval from diagnosis of metastatic disease to inclusion. All statistical tests were two-sided. **b**, Kaplan–Meier plot of PFS per cohort in the FAS population ($n = 177$). The median PFS was 11.1 months (95% CI 8.5–14.4) in cohort 1, 6.7 months (95% CI 4.4–8.3) in cohort 2 and 4.2 months (95% CI 2.0–5.7) in cohort 3. PFS was longer in cohort 1 (adjusted HR: 0.53, 95% CI 0.34–0.84, $P = 0.007$) and shorter in cohort 3 (adjusted HR: 1.96, 95% CI 1.21–3.15, $P = 0.006$) compared to cohort 2. The adjusted HR and P value were derived from a multivariable Cox proportional hazard model taking as reference cohort 2 and adjusted to the same variables used for the confirmed objective response. All statistical tests were two-sided.

Primary outcome results

In total, 177 patients were included in the full analysis set (FAS) (Fig. 1). The median number of cycles of T-DXd was 12.5 (range, 2–31) in cohort 1, 10 (range, 1–29) in cohort 2 and six (range, 1–26) in cohort 3. The primary endpoint of the study was the confirmed objective response rate (ORR). As of the 19 October 2021 data cutoff, a confirmed objective response occurred in 86 (48.6%) patients: 48 patients (70.6%, 95% CI 58.3–81) in cohort 1 (primary endpoint met), 27 patients (37.5%, 95% CI 26.4–49.7) in cohort 2 (primary endpoint met) and 11 patients (29.7%, 95% CI 15.9–47) in cohort 3 (primary endpoint inconclusive) (Fig. 2a). In addition, seven patients presented an unconfirmed objective response (3.9%). When we looked at the best tumor shrinkage of target lesions, we observed a median reduction of –57.2% (range, –100 to 13.6), –25.3% (range, –100 to 203.2) and –12.5% (range, –80.6 to 68.7) in cohorts 1, 2 and 3, respectively ($P < 0.0001$). In addition, we evaluated the association between confirmed objective response and cohorts adjusting for clinical characteristics listed in the Methods. Patients from cohort 1 presented a higher likelihood of confirmed objective response as compared to cohort 2 (adjusted odds ratio (OR): 3.96, 95% CI 1.78–8.77, $P = 0.001$). The likelihood of confirmed objective response was not significantly different between cohort 3 and cohort 2 (adjusted OR: 0.63, 95% CI 0.25–1.54, $P = 0.30$). We also investigated whether the association between clinical characteristics and confirmed OR differed by cohort. The presence of ≥ 3 metastatic sites at screening was the only parameter significantly associated with non-response in cohort 2 ($P = 0.018$). Then, we assessed the confirmed ORR in patients who presented a change

in the HER2 status of the baseline biopsy as compared to routine care. Among the 14 patients presenting a HER2 overexpression on sample from routine care and who were finally assigned to cohort 2 (HER2-low) after biopsy at baseline, six presented a confirmed objective response (42.9%, 95% CI 17.7–71.1). Confirmed ORRs were 19% (95% CI 5.4–41.9, $n = 4/21$) in patients with HER2 non-expressing mBC who were assigned to cohort 2 (HER2-low) after baseline biopsy and 40% (95% CI 12.2–73.8, $n = 4/10$) in patients with HER2 expression (overexpressed or low) who were assigned to cohort 3 (IHC 0) after baseline biopsy.

We observed a similar confirmed ORR between patients with HER2 IHC 1+ and IHC 2+/ERBB2 ISH-negative in cohort 2 (Extended Data Fig. 3).

Secondary outcome results

The secondary endpoints were duration of response, PFS, OS, clinical benefit rate and safety. In 93 patients with a confirmed or unconfirmed objective response, the median duration of response was 9.7 months (95% CI 6.8–13) in cohort 1, 7.6 months (95% CI 4.2–9.2) in cohort 2 and 6.8 months (95% CI 2.8–not reached) in cohort 3. After a median follow-up of 15.6 months (95% CI 12.6–16.7), the median PFS was 11.1 months (95% CI 8.5–14.4) in cohort 1, 6.7 months (95% CI 4.4–8.3) in cohort 2 and 4.2 months (95% CI 2.0–5.7) in cohort 3. In the multivariable analysis adjusted for clinical characteristics, cohort 1 was associated with longer PFS (adjusted HR: 0.53, 95% CI 0.34–0.84, $P = 0.007$) and cohort 3 with shorter PFS (adjusted HR: 1.96, 95% CI 1.21–3.15, $P = 0.006$) as compared to cohort 2 (Fig. 2b). When we assessed the association

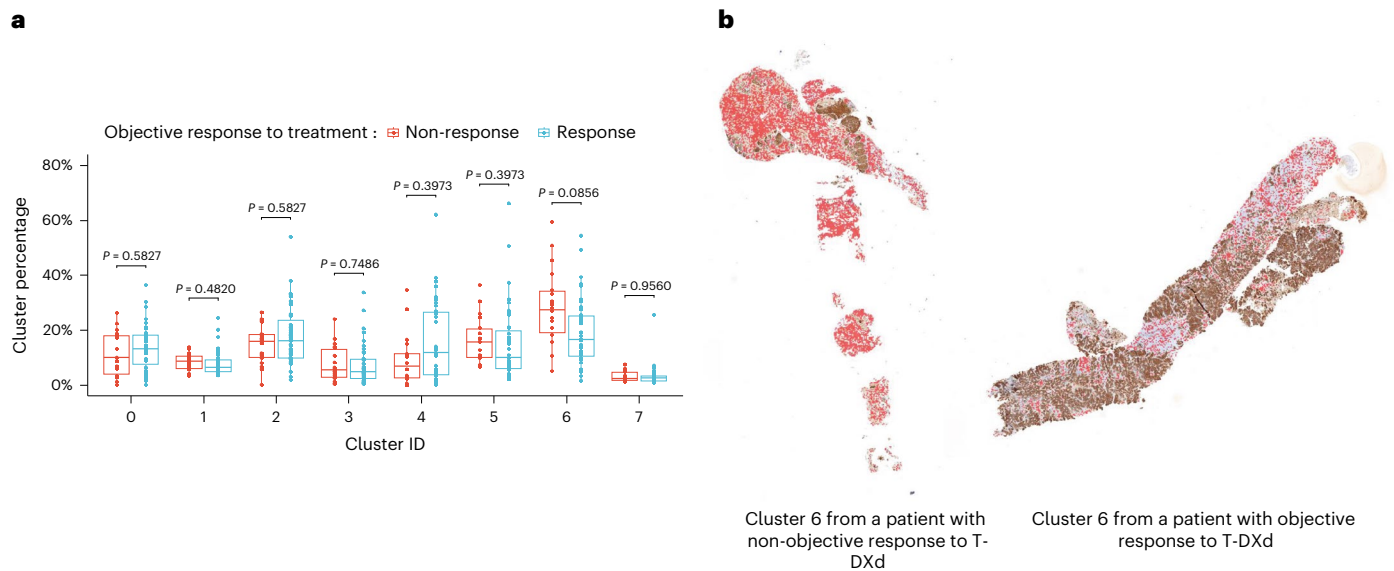


Fig. 3 | HER2 expression patterns and treatment response. a, Clusters' relative percentage according to T-DXd sensitivity in cohort 1 (HER2-overexpressing). For each patient, the corresponding HER2 pathology slide ($n = 61$) was divided into 64×64 -px non-overlapping patches that were classified into eight clusters using a Mini-Batch K -means algorithm. The following box plot illustrates the relative percentage of each cluster in each slide and its association with the confirmed objective response or non-response to T-DXd. Box center lines, box ranges, whiskers and dots indicate medians, quartiles, $1.5 \times$ IQR and outliers, respectively. Cluster 6 presented a significant association with non-response

to T-DXd ($P = 0.011$, FDR-adjusted $P = 0.086$). P values were calculated using the Mann–Whitney U -test and adjusted for multiple hypothesis testing using the Benjamini–Hochberg method. All statistical tests were two-sided. **b**, One pair of pathology slides that shows cluster 6 in red. A patient with resistance (left) and sensitivity (right) to T-DXd. Cluster 6 comprised HER2-negative areas with moderate cell density (mean value of 30% (95% CI 25–34)), containing mainly fibroblasts and immune cells (mean value of 56% (95% CI 50–62) and 27% (95% CI 22–32), respectively).

between clinical characteristics and PFS by cohort, we found that an interval from diagnosis of metastatic disease to inclusion of more than 24 months was associated with a longer PFS (HR 24–60 months versus 0–24 months: 0.35, 95% CI 0.16–0.79; HR >60 months versus 0–24 months: 0.24, 95% CI 0.10–0.57; $P = 0.002$) in cohort 1; the presence of ≥ 3 metastatic sites at screening with a shorter PFS (HR: 2.24, 95% CI 1.27–3.93, $P = 0.004$) and HR expression with a longer PFS (HR: 0.48, 95% CI 0.26–0.92, $P = 0.022$) in cohort 2. Finally, an ECOG performance status of 1 at screening was associated with a shorter PFS (HR: 2.13, 95% CI 1.02–4.44, $P = 0.037$) in cohort 3. A similar PFS was observed between patients with HER2 IHC 1+ and IHC 2+/ERBB2 ISH-negative in cohort 2 (Extended Data Fig. 4). PFS for each cohort according to HR status is described in Supplementary Fig. 1. After a median follow-up of 14.1 months (95% CI 13.2–15.2), the median OS was not reached (95% CI 16.7–not reached) in cohort 1, not reached (95% CI 11.5–not reached) in cohort 2 and 11.6 months (95% CI 8.3–17.3) in cohort 3. The clinical benefit rate was 85.3% (95% CI 74.6–92.7) in cohort 1, 56.9% (95% CI 44.7–68.6) in cohort 2 and 35.1% (95% CI 20.2–52.5) in cohort 3.

In total, 145 patients (81%) permanently discontinued treatment: 49 (72.1%) in cohort 1, 61 (83.6%) in cohort 2 and 35 (92.1%) in cohort 3. The reason for discontinuation was disease progression in 125 (86.2%) patients and toxicity in 13 (9%) patients. Adverse events were consistent with previous data¹⁰ and are reported in Extended Data Tables 1 and 2. The most common adverse effects \geq grade 3 were neutropenia (12%), fatigue (8%) and vomiting (6%), consistent with the toxicity profile of TOP1 inhibitors. Nine patients (5%) presented interstitial lung disease or pneumonitis, all of them grade 1 or grade 2. Three patients (1.7%) presented ejection fraction decreased (one grade 3). Three patients (1.7%) presented a grade 5 adverse effect.

HER2 expression patterns and treatment response

We further examined HER2 expression patterns in the three cohorts as an exploratory objective. We first assessed whether HER2

spatial distribution predicts drug response in patients from cohort 1 (HER2-overexpressing mBC; $n = 61$) (Extended Data Fig. 5). Machine learning analyses indicated that HER2 slides could be segmented into eight clusters using an unsupervised clustering algorithm (Extended Data Fig. 6). Intensity of diaminobenzidine (DAB) staining (HER2 expression) and cell density were two core features that drove the unsupervised clustering (Supplementary Fig. 2). We compared non-responders to responders based on the percentage of each of the eight identified clusters, finding that non-responders had a greater percentage of cluster 6 in their tumor ($P = 0.011$, false discovery rate (FDR)-adjusted $P = 0.086$), with no other cluster showing a statistically significant difference among groups (Fig. 3). Cluster 6 was characterized by a low HER2 staining (median, 0.19; interquartile range (IQR), 0.10–0.47) and a moderate cell density (37% of patches without cells and 34% with one nucleus). Cells present in cluster 6 patches were mainly fibroblasts and immune cells (mean value of 56% (95% CI 50–62) and 27% (95% CI 22–32), respectively). In 28 of 60 (47%) patients, cluster 6 also contained tumor cells with a mean value of 40% (95% CI 24–56), 48% (95% CI 33–63) and 12% (95% CI 0–23) of HER2 IHC 0, IHC 1+ and IHC 2+, respectively (Supplementary Table 1). We then used this model to analyze 65 HER2 pathology slides from cohort 2 (HER2-low mBC; Extended Data Fig. 5). No significant association with T-DXd efficacy was observed (Supplementary Fig. 3). Next, we trained a new model using data from 65 patients from cohort 2 (HER2-low mBC; Methods) (Extended Data Fig. 5). We did not find a significant association between the identified clusters and T-DXd response (Supplementary Fig. 4).

We then assessed whether levels of HER2 expression could predict drug response in patients from cohort 3 (HER2 IHC 0, $n = 37$). We first evaluated *ERBB2* gene expression by reverse transcription polymerase chain reaction (RT–PCR) in 24 tumor samples obtained at baseline with $\geq 30\%$ of tumor cells (Extended Data Fig. 7). We found that 5 of 14 (35.7%, 95% CI 12.8–64.9) patients with *ERBB2* expression below the median presented a confirmed objective response

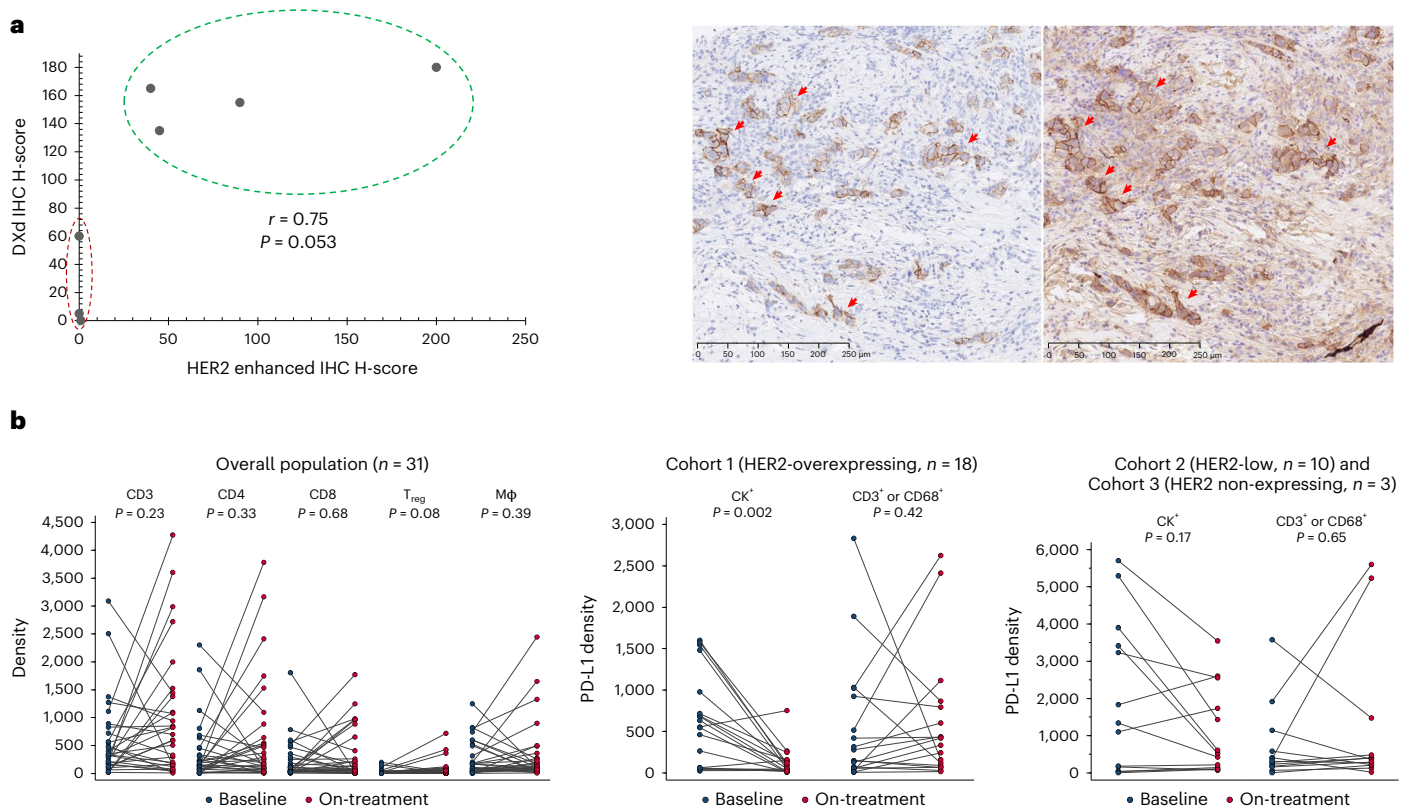


Fig. 4 | Mechanisms of action of T-DXd. a, Illustration of the correlation between T-DXd distribution and HER2 expression. T-DXd was determined by IHC using an Ac anti-DXd (H-score) and HER2 by an enhanced protocol of IHC (H-score) in seven paired samples at baseline and during treatment. The staining was performed in one sample per case. The correlation was calculated by Pearson correlation coefficient, which showed a moderate correlation ($r = 0.75$, $P = 0.053$). P value was calculated using a two-sided Pearson correlation test. On the bottom, a pathology slide that shows HER2 staining (red arrows) on the left and T-DXd staining (red arrows) on the right. **b**, Illustration of the immune microenvironment modulation by T-DXd. Tumor biopsies at baseline and days 22–43 after cycle 1 of T-DXd were assessed by multiplex immunofluorescence

($n = 31$). No quantitative modulation of the immune microenvironment by T-DXd in the overall population ($n = 31$) was observed. There was a significant decrease in PD-L1 expression presumably due to the cytotoxic effect of T-DXd on tumor cells ($CK^+/PD-L1^+$) in patients with HER2-overexpressing mBC ($n = 18$, $P = 0.002$). Immune cells, represented by $CD3^+/PD-L1^+$ or $CD68^+/PD-L1^+$, did not show a decrease during treatment in cohort 1 ($n = 18$, $P = 0.42$). No significant decrease of PD-L1⁺ tumor ($P = 0.17$) or immune cells ($P = 0.65$) was observed in patients with HER2-low and HER2-non-expressing mBC ($n = 13$) during treatment. Blue bullets and red bullets represent at-baseline and on-treatment samples, respectively. P values were calculated using the Wilcoxon matched-pairs signed-rank test. All statistical tests were two-sided. Mφ, macrophage; T_{reg}, regulatory T cell.

as compared to 3 of 10 patients (30%, 95% CI 6.7–65.2) with *ERBB2* expression above the median. HER2-stained slides obtained at baseline biopsy from 31 patients in cohort 3 were reviewed by two pathologists (Extended Data Fig. 7). Some level of HER2 expression was detected in 15 samples (8 ‘ultra-low’ (defined in the Methods section) and 7 IHC 1+). A confirmed objective response was observed in 6 of 15 (40%, 95% CI 16.3–67.7) patients with detectable HER2 expression and in 4 of 16 (25%, 95% CI 7.3–52.4) patients without detectable HER2 expression.

T-DXd mechanisms of action

We further explored T-DXd distribution (exploratory objective) in seven paired biopsies obtained at baseline and during treatment (Extended Data Fig. 7). Tumor cells with a high level of HER2 expression presented strong T-DXd staining (Fig. 4a). Conversely, three samples classified HER2 IHC 0 by an enhanced protocol (Methods) presented no or very few T-DXd staining (Pearson correlation coefficient $r = 0.75$, $P = 0.053$). Two of these three patients with low level of T-DXd distribution presented a confirmed partial response with a PFS of 17.8 months (censored patient) and 12 months, respectively. We then investigated whether T-DXd modulates the immune microenvironment (exploratory objective) in 31 patients from the three cohorts (Extended Data Fig. 7). No quantitative modulation of immune cells by T-DXd was detected

at week 3 or week 6 after drug administration (Fig. 4b). A significant decrease in PD-L1 expression was observed in patients in cohort 1 ($n = 18$, $P = 0.002$), presumably due to the cytotoxic effect of T-DXd on tumor cells (cytokeratin (CK)⁺/programmed death-ligand 1 (PD-L1)⁺) (Fig. 4b). A decrease in tumor-cell-proximate macrophages (0–10 μm) was also observed in cohort 1 ($n = 18$, FDR-adjusted $P = 0.0305$; Extended Data Fig. 8).

Mechanisms of resistance to T-DXd

To identify mechanisms of primary and secondary resistance (exploratory objective), we performed whole-exome sequencing (WES) of frozen tumor tissue obtained at baseline ($n = 89$: 38 from cohort 1; 37 from cohort 2; and 14 from cohort 3) and at resistance ($n = 21$: five from cohort 1, 11 from cohort 2 and five from cohort 3). Eleven biopsies at resistance were matched with baseline biopsies (Extended Data Fig. 7). Figure 5a reports the driver somatic mutations and copy number alterations (CNAs) at baseline according to sensitivity to T-DXd. With the exception of *ERBB2* amplifications, we did not observe a significant association between driver alterations and upfront resistance (FDR-adjusted $P > 0.54$). *ERBB2* hemizygous deletion was detected in six of 89 (7%) patients at baseline. Interestingly, four of these patients did not respond to T-DXd (three in cohort 2 and one in cohort 3). We next explored which genomic alterations were acquired at resistance

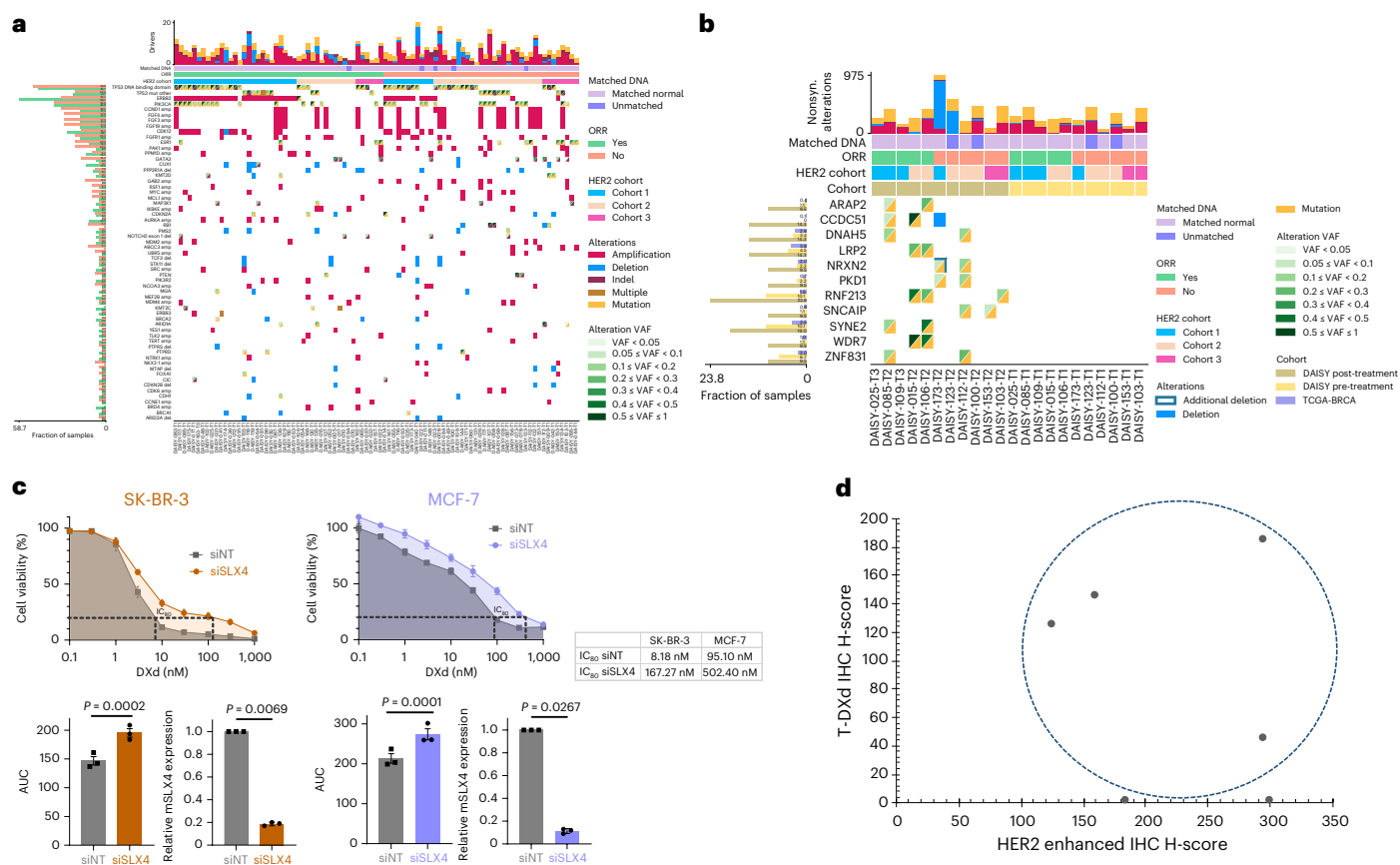


Fig. 5 | Mechanisms of resistance to T-DXd. a, Oncoplot of driver mutations and CNAs identified in at least 3% of tumor biopsies at baseline ($n = 89$). Blood samples were available for analyses in 84 patients. If a gene has at least one driver mutation or CNA in at least 3% of pretreatment biopsies, any other driver alteration of the same gene is shown, regardless of its frequency. **b**, Oncoplot of acquired genomic alterations identified at resistance ($n = 11$). Eleven biopsies at resistance (on the left) were matched with pretreatment biopsies (on the right) from the same patient. Only genes that were not altered in any of the 11 pretreatment samples and that acquired an alteration in at least two samples at resistance (three samples in case all events were CNAs) are shown. The left histogram depicts the frequency at which the gene was altered in the

pretreatment ($n = 89$), resistance ($n = 21$) and TCGA-BRCA ($n = 684$) cohorts for comparison. **c**, Dose-response survival curves of SK-BR-3 and MCF-7 cell lines transfected with non-targeting or *SLX4*-targeted siRNAs (siNT or siSLX4, respectively) and exposed to DXd at the indicated doses for 5 days. Area under the curve (AUC) and IC_{80} values were determined for each condition. Data are mean surviving fractions ± s.e.m., $n = 3$ experiments for both cell lines. Statistical analysis was performed using Welch's t -test (two-tailed). **d**, Illustration of T-DXd uptake and HER2 expression at resistance ($n = 6$). T-DXd was determined by IHC using an Ac anti-DXd (H-score) and HER2 by an enhanced protocol of IHC (H-score). T-DXd was observed in four of six patients whose biopsy at resistance was done ≤ 6 weeks after last T-DXd infusion.

by comparing the genomic landscape of 11 pairs of biopsies obtained at baseline and at resistance. We found that 11 genes presented an alteration acquired at resistance in at least 2 of 11 pairs while not being mutated in any of the 11 matched baseline samples (Fig. 5b). Three of twenty-one (14%) samples obtained at resistance to T-DXd presented a *SLX4* mutation: one of them was not observed in the matched baseline sample; the second one was present in the biopsy at baseline; and, for the third one, the biopsy at baseline was not available. Two of these mutations were ranked as deleterious according to CADD and SIFT; however, no evidence of loss of second allele was found. *SLX4* M1591L was observed in the post-treatment sample of DAISY-109 patient. Detailed investigations of the mutation filtering performed by the variant caller (Methods) revealed that the mutation is incorrectly flagged in the baseline sample due to the presence of three nearby artifactual mutations. Additionally, rs149126845 missense variant (*SLX4* K458E) was detected in the post-treatment sample DAISY-098-T2, but, due to the absence of a matched blood sample and relatively high frequency of this mutation in the Genome Aggregation Database (gnomAD), we decided not to include this variant. Conversely, *SLX4* mutations were present in three of 89 (3%) pretreatment biopsies and 1.5% in The Cancer Genome Atlas (TCGA) breast cancer (BRCA). We assessed cell viability

in two breast cancer cell lines depleted for *SLX4* and treated with different doses of DXd for 5 days. DXd concentration needed to achieve 80% inhibition (IC_{80}) was increased 20-fold (8.18 nM versus 167.27 nM) in *SLX4*-silenced SK-BR-3 cells and fivefold (95.1 nM versus 502.4 nM) in *SLX4*-silenced MCF-7 cells (Fig. 5c).

Finally, we investigated how HER2 expression and T-DXd distribution were modulated at resistance as compared to pretreatment (Extended Data Fig. 7). Thirteen of 20 (65%, 95% CI 40.8–84.6) patients presented a decrease of HER2 tumor expression after resistance to the drug, namely three IHC 3+ (two to IHC 2+ and one to IHC 1+), six IHC 2+ (three to IHC 1+ and three to IHC 0) and four from IHC 1+ to IHC 0. Intratumoral uptake of T-DXd was observed in four of six patients from cohort 1 at resistance (biopsy within 6 weeks after last infusion), suggesting that T-DXd can still be distributed to cancer cells in a subset of patients at resistance (Fig. 5d). All patients presenting tumoral uptake of T-DXd at resistance had HER2 IHC 3+ or 2+ on biopsy done at resistance.

Discussion

We report converging evidence that HER2 expression is a determinant of T-DXd efficacy. Specifically, the PFS rates were significantly different

across the three cohorts of patients; T-DXd uptake was different according to HER2 levels; and HER2 expression decreased at resistance. A previous study suggested that HER2 quantitative continuous score (QCS) could potentially predict outcome to T-DXd in patients with HER2-low mBC¹⁵. Previous clinical trials showed that tumor responses were similar in HER2 IHC 1+ and IHC 2+ subgroups^{14,16}. This finding was confirmed in the DAISY trial, suggesting that IHC may not be the optimal test to define the boundary of HER2 expression to predict efficacy in patients with HER2-low mBC.

Although T-DXd anti-tumor activity increased when HER2 expression was high, modest anti-tumor activity was also observed in patients with HER2 IHC 0. This suggests that very low levels of HER2 could allow uptake of T-DXd and/or that drug efficacy could be partially mediated by HER2-independent mechanisms. A study that involved 18 pathologists showed a low level of concordance (26%) to score HER2 IHC 0 and 1+ (ref. 17). In our study, 48% ($n = 15$) of HER2 slides IHC 0 had detectable HER2 expression, either 'ultra-low' or IHC 1+, in an external pathology review. In another study¹⁸, 67% of 364 breast cancer cases classified HER2 IHC 0 had detectable HER2 expression by using quantitative immunofluorescence. Collectively, these studies suggest that HER2 IHC 0 includes a large number of cancers with some level of HER2 expression and that a subset of these patients is sensitive to T-DXd. This provides a strong rationale for ongoing trials such as DB-06, testing efficacy of T-DXd in patients with HER2 'ultra-low' mBC¹⁹. This may expand the population deriving benefit from T-DXd and outlines the importance of the emergence of optimized HER2 assays. Notably, we did not detect any efficacy difference based on *ERBB2* gene expression within the group of patients with HER2 IHC 0 mBC, further suggesting potential drug activity in patients with very low, if any, expression of *ERBB2*. The presence of free payload, after cleavage of T-DXd linker, could be another possible explanation for T-DXd efficacy in patients with HER2 IHC 0 mBC²⁰. The assessment of efficacy according to *ERBB2* gene expression in patients with HER2-low mBC (IHC 1+ or IHC 2+/ISH-negative) will be performed in the future. We decided not to conduct this analysis initially, as a previous report suggested that *ERBB2* mRNA levels showed little inter-patient variability in HER2-non overexpressing BC²¹. In addition, similar efficacy was observed in HER2 1+ versus HER2 2+/ISH-negative mBC.

Although numbers are small and should be interpreted cautiously, the confirmed objective response was slightly lower in patients with HER2-overexpressing mBC who became HER2-low after baseline biopsy. This finding could be relevant to interpret the DB-02 and DB-03 studies where patients received multiple lines of prior anti-HER2 therapies.

While efficacy of second-generation ADCs, such as T-DM1, was strongly associated with target expression²², this has not been shown with the latest generation of ADCs. For example, TROP2 expression was not predictive for the efficacy of the TROP2-targeting ADC sacituzumab govitecan in the ASCENT trial, although the number of patients with TROP2-low expression was small, and the analyses did not allow definitive conclusion²³. Efficacy of patritumab deruxtecan was observed across patients with mBC with a broad spectrum of HER3 expression^{24,25}, although most exhibited high levels of HER3 tumor expression.

We observed a lower median PFS in the DAISY trial than in previously reported studies testing the efficacy of T-DXd. PFS was longer in the DB-02 (ref. 12) trial than in the DAISY trial (17.8 months versus 11.1 months). This could be explained by a lower number of prior therapies (median of two previous lines of therapy in metastatic setting) and a better general condition as measured by the ECOG performance status at inclusion (ECOG performance status = 0: 56% versus 31%) in DB-02. The DB-01 trial also showed longer PFS as compared to our study (19.4 months)¹¹. The reasons for this difference are unclear. In DB-01, 50% of patients were in good general condition (ECOG performance status = 0). However, patients were as heavily pretreated

as in the DAISY trial (median of six previous lines of therapy in metastatic setting). Efficacy results from DB-03 are not directly comparable to our study because patients did not receive prior T-DM1 (ref. 26). In the population of patients with HER2-low mBC, the median PFS was slightly higher in the DB-04 trial¹⁴ as compared to our study (9.9 months versus 6.7 months). The proportion of patients with hormone receptor-positive breast cancer (89% versus 79%), the general condition (ECOG performance status = 0: 54% versus 45%) and the number of prior therapies (median of three previous lines of therapy in metastatic setting in DB-04) were different between the two studies and could explain the difference in outcome.

The safety profile of T-DXd in our study was similar to previous reports^{11,14}. The most common adverse effects \geq grade 3 were neutropenia, fatigue and vomiting, consistent with that of TOP1 inhibitors. Most cases of interstitial lung disease or pneumonitis and decreased ejection fraction in this trial were mild or moderate, and the overall incidence was consistent with the ones reported in previous studies^{14,27}.

Preclinical data showed that T-DXd increased tumor-infiltrating dendritic cells and CD8⁺ T cells in an immunocompetent mouse model inoculated with human HER2-expressing colon cancer cells²⁸. Based on these data, several clinical trials assessing T-DXd in combination with immune checkpoint inhibitors are ongoing^{29,30}. Our study did not validate these findings, but there was no decrease of CD8⁺ T cells, in contrast to previous observations with systemic chemotherapy³¹.

Although HER2 expression substantially decreased at the time of resistance to T-DXd, there is no robust evidence that a reduction of T-DXd uptake is the dominant mechanism of resistance in the present study. Indeed, T-DXd was still distributed in the cancer cells in four of six patients at the time of resistance. Unfortunately, no quantitative comparison of T-DXd uptake could be done during treatment and at resistance. In a case report, resistance to sacituzumab govitecan, an ADC targeting TROP2, was associated with *TROP2* mutation and defective plasma membrane localization³², suggesting that the ADC target could be involved in resistance. We identified mutations of *SLX4* at resistance in three of 21 (14%) patients. *SLX4* encodes a DNA repair protein that regulates structure-specific endonucleases and might have a role in resistance to TOP1 inhibition^{33,34}. The TCGA reports *SLX4* mutations in 1.5% of primary breast cancer, the majority hormone receptor-positive/HER2-negative ductal carcinoma³⁵. Another study reported *SLX4* mutations in 1.3% of HER2-negative mBC (50% hormone receptor-positive)³⁶. Although corroborated with in vitro studies, the nature of *SLX4* mutations found in the DAISY trial remains to be determined. In contrast to previous data, we did not detect *TOP1* mutations at the time of resistance³².

Our trial has several limitations. We did not include negative controls for HER2 expression assessment at resistance; the number of samples analyzed was small; and there was no validation cohort for several of the translational objectives.

The present study suggests that HER2 is a determinant of sensitivity to T-DXd, although modest anti-tumor activity was also observed in a small subset of patients whose cancer did not express HER2, suggesting other mechanisms of action. Resistance to T-DXd may occur at different levels, potentially involving decrease of HER2 expression, alterations of the cytotoxic effect of DXd and the tumor microenvironment. These data indicate that precision medicine approaches based on molecular analyses will be necessary to optimize treatment after resistance to T-DXd.

Online content

Any methods, additional references, Nature Portfolio reporting summaries, source data, extended data, supplementary information, acknowledgements, peer review information; details of author contributions and competing interests; and statements of data and code availability are available at <https://doi.org/10.1038/s41591-023-02478-2>.

References

- Sung, H. et al. Global Cancer Statistics 2020: GLOBOCAN estimates of incidence and mortality worldwide for 36 cancers in 185 countries. *CA Cancer J. Clin.* **71**, 209–249 (2021).
- Malmgren, J. A., Mayer, M., Atwood, M. K. & Kaplan, H. G. Differential presentation and survival of de novo and recurrent metastatic breast cancer over time: 1990–2010. *Breast Cancer Res. Treat.* **167**, 579–590 (2018).
- Grinda, T. et al. Evolution of overall survival and receipt of new therapies by subtype among 20 446 metastatic breast cancer patients in the 2008–2017 ESME cohort. *ESMO Open* **6**, 100114 (2021).
- National Cancer Institute. Surveillance, Epidemiology, and End Results Program. Cancer Stat Facts: Female Breast Cancer. <https://seer.cancer.gov/statfacts/html/breast.html>
- Cancer Genome Atlas Network. Comprehensive molecular portraits of human breast tumours. *Nature* **490**, 61–70 (2012).
- Swain, S. M. et al. Pertuzumab, trastuzumab, and docetaxel in HER2-positive metastatic breast cancer. *N. Engl. J. Med.* **372**, 724–734 (2015).
- Ogitani, Y., Hagihara, K., Oitate, M., Naito, H. & Agatsuma, T. Bystander killing effect of DS-8201a, a novel anti-human epidermal growth factor receptor 2 antibody–drug conjugate, in tumors with human epidermal growth factor receptor 2 heterogeneity. *Cancer Sci.* **107**, 1039–1046 (2016).
- Junttila, T. T., Li, G., Parsons, K., Phillips, G. L. & Sliwkowski, M. X. Trastuzumab-DM1 (T-DM1) retains all the mechanisms of action of trastuzumab and efficiently inhibits growth of lapatinib insensitive breast cancer. *Breast Cancer Res. Treat.* **128**, 347–356 (2011).
- Verma, S. et al. Trastuzumab emtansine for HER2-positive advanced breast cancer. *N. Engl. J. Med.* **367**, 1783–1791 (2012).
- Cortés, J. et al. Trastuzumab deruxtecan versus trastuzumab emtansine for breast cancer. *N. Engl. J. Med.* **386**, 1143–1154 (2022).
- Modi, S. et al. Abstract PD3-06: Updated results from DESTINY-breast01, a phase 2 trial of trastuzumab deruxtecan (T-DXd) in HER2 positive metastatic breast cancer. *Cancer Res.* **81**, PD3-06 (2021).
- André, F. et al. Trastuzumab deruxtecan versus treatment of physician's choice in patients with HER2-positive metastatic breast cancer (DESTINY-Breast02): a randomised, open-label, multicentre, phase 3 trial. *Lancet* **401**, 1773–1785 (2023).
- Cardoso, F. et al. 5th ESO-ESMO international consensus guidelines for advanced breast cancer (ABC 5). *Ann. Oncol.* **31**, 1623–1649 (2020).
- Modi, S. et al. Trastuzumab deruxtecan in previously treated HER2-low advanced breast cancer. *N. Engl. J. Med.* **387**, 9–20 (2022).
- Gustavson, M. et al. Abstract PD6-01: Novel approach to HER2 quantification: digital pathology coupled with AI-based image and data analysis delivers objective and quantitative HER2 expression analysis for enrichment of responders to trastuzumab deruxtecan (T-DXd; DS-8201), specifically in HER2-low patients. *Cancer Res.* **81**, PD6-01 (2021).
- Modi, S. et al. Antitumor activity and safety of trastuzumab deruxtecan in patients with HER2-low-expressing advanced breast cancer: results from a phase Ib study. *J. Clin. Oncol.* **38**, 1887–1896 (2020).
- Fernandez, A. I. et al. Examination of low ERBB2 protein expression in breast cancer tissue. *JAMA Oncol.* **8**, 607–610 (2022).
- Moutafi, M. et al. Quantitative measurement of HER2 expression to subclassify *ERBB2* unamplified breast cancer. *Lab. Invest.* **102**, 1101–1108 (2022).
- A phase 3, randomized, multi-center, open-label study of trastuzumab deruxtecan (T-DXd) versus investigator's choice chemotherapy in HER2-low, hormone receptor positive breast cancer patients whose disease has progressed on endocrine therapy in the metastatic setting (DESTINY-Breast06). <https://clinicaltrials.gov/ct2/show/NCT04494425>
- Colombo, R. & Rich, J. R. The therapeutic window of antibody drug conjugates: a dogma in need of revision. *Cancer Cell* **40**, 1255–1263 (2022).
- Gong, Y. et al. Determination of oestrogen-receptor status and ERBB2 status of breast carcinoma: a gene-expression profiling study. *Lancet Oncol.* **8**, 203–211 (2007).
- Baselga, J. et al. Relationship between tumor biomarkers and efficacy in EMILIA, a phase III study of trastuzumab emtansine in HER2-positive metastatic breast cancer. *Clin. Cancer Res.* **22**, 3755–3763 (2016).
- Bardia, A. et al. Biomarker analyses in the phase III ASCENT study of sacituzumab govitecan versus chemotherapy in patients with metastatic triple-negative breast cancer. *Ann. Oncol.* **32**, 1148–1156 (2021).
- Krop, I. E. et al. Results from the phase 1/2 study of patritumab deruxtecan, a HER3-directed antibody–drug conjugate (ADC), in patients with HER3-expressing metastatic breast cancer (MBC). *J. Clin. Oncol.* https://doi.org/10.1200/JCO.2022.40.16_suppl.1002 (2022).
- Prat, A. et al. Patritumab deruxtecan (HER3-DXd) in early-stage HR⁺/HER2⁻ breast cancer: final results of the SOLTI TOT-HER3 window of opportunity trial. *Ann. Oncol.* **33**, S165–S174 (2022).
- Hurvitz, S. A. et al. Trastuzumab deruxtecan versus trastuzumab emtansine in patients with HER2-positive metastatic breast cancer: updated results from DESTINY-Breast03, a randomised, open-label, phase 3 trial. *Lancet* **401**, 105–117 (2023).
- Hurvitz, S. A. et al. Trastuzumab deruxtecan versus trastuzumab emtansine in patients with HER2-positive metastatic breast cancer: updated survival results of the randomized, phase 3 study DESTINY-Breast03. 2022 San Antonio Breast Cancer Symposium. Abstract GS2-O (2022).
- Iwata, T. N. et al. A HER2-targeting antibody–drug conjugate, trastuzumab deruxtecan (DS-8201a), enhances antitumor immunity in a mouse model. *Mol. Cancer Ther.* **17**, 1494–1503 (2018).
- Schmid, P. et al. BEGONIA: phase 1b/2 study of durvalumab (D) combinations in locally advanced/metastatic triple-negative breast cancer (TNBC)—initial results from arm 1, d+paclitaxel (P), and arm 6, d+trastuzumab deruxtecan (T-DXd). *J. Clin. Oncol.* **39**, 1023–1023 (2021).
- Borghaei, H. et al. Trastuzumab deruxtecan (T-DXd; DS-8201) in combination with pembrolizumab in patients with advanced/metastatic breast or non-small cell lung cancer (NSCLC): a phase Ib, multicenter, study. *J. Clin. Oncol.* **38**, TPS1100(2020).
- Verma, R. et al. Lymphocyte depletion and repopulation after chemotherapy for primary breast cancer. *Breast Cancer Res.* **18**, 10 (2016).
- Coates, J. T. et al. Parallel genomic alterations of antigen and payload targets mediate polyclonal acquired clinical resistance to sacituzumab govitecan in triple-negative breast cancer. *Cancer Discov.* **11**, 2436–2445 (2021).
- Svendsen, J. M. et al. Mammalian BTBD12/SLX4 assembles a Holliday junction resolvase and is required for DNA repair. *Cell* **138**, 63–77 (2009).
- Garner, E., Kim, Y., Lach, F. P., Kottmann, M. C. & Smogorzewska, A. Human GEN1 and the SLX4-associated nucleases MUS81 and SLX1 are essential for the resolution of replication-induced Holliday junctions. *Cell Rep.* **5**, 207–215 (2013).

35. National Cancer Institute. Center for Cancer Genomics. The Cancer Genome Atlas Program (TCGA). <https://www.cancer.gov/about-nci/organization/ccg/research/structural-genomics/tcga>
36. Bertucci, F. et al. Genomic characterization of metastatic breast cancers. *Nature* **569**, 560–564 (2019).

Publisher's note Springer Nature remains neutral with regard to jurisdictional claims in published maps and institutional affiliations.

Open Access This article is licensed under a Creative Commons Attribution 4.0 International License, which permits use, sharing, adaptation, distribution and reproduction in any medium or format,

as long as you give appropriate credit to the original author(s) and the source, provide a link to the Creative Commons license, and indicate if changes were made. The images or other third party material in this article are included in the article's Creative Commons license, unless indicated otherwise in a credit line to the material. If material is not included in the article's Creative Commons license and your intended use is not permitted by statutory regulation or exceeds the permitted use, you will need to obtain permission directly from the copyright holder. To view a copy of this license, visit <http://creativecommons.org/licenses/by/4.0/>.

© The Author(s), under exclusive licence to Springer Nature America, Inc. 2023

¹INSERM U981, Gustave Roussy, Villejuif, France. ²Department of Medical Oncology, Gustave Roussy, Villejuif, France. ³Department of Medical Oncology, CHU Dupuytren, Limoges, France. ⁴Department of Biostatistics, Institut Claudius-Regaud, IUCT Oncopole, Toulouse, France. ⁵CVN Lab, CentraleSupélec, Université Paris-Saclay, Gif-Sur-Yvette, France. ⁶OPIS, Inria, CentraleSupélec, Université Paris-Saclay, Gif-Sur-Yvette, France. ⁷MICS Lab, CentraleSupélec, Université Paris-Saclay, Gif-Sur-Yvette, France. ⁸Department of Medical Oncology, Centre Antoine Lacassagne, Nice, France. ⁹Department of Medical Oncology, Centre Léon Bérard, Lyon, France. ¹⁰Department of Medical Oncology, Centre Paoli Calmettes, Marseille, France. ¹¹Department of Medical Oncology, Centre François Baclesse, Caen, France. ¹²AMMICA Platform, INSERM US23, CNRS UAR 3655, AMMICA, Villejuif, France. ¹³Imaging and Cytometry Platform, Gustave Roussy, UAR 23/3655, Université Paris-Saclay, Villejuif, France. ¹⁴Department of Medical Biology and Pathology, Gustave Roussy, Villejuif, France. ¹⁵Translational Research Department, Daiichi Sankyo RD Novare, Tokyo, Japan. ¹⁶R&D Department, Unicancer, Paris, France. ¹⁷UMR9019, CNRS, Gustave Roussy, Université Paris-Saclay, Villejuif, France. ¹⁸Department of Medical Oncology, Centre Eugène Marquis, Rennes, France. ¹⁹Faculty of Medicine, Université Paris-Saclay, Kremlin Bicêtre, France. ²⁰These authors contributed equally: Elise Deluche, Amelie Lusque, Loïc Le-Bescond, Magali Lacroix-Triki, Veronique Diéras, Fabrice André. ✉ e-mail: fabrice.andre@gustaveroussy.fr

Methods

Patients and study design

DAISY (NCT04132960) is a prospective, phase 2, open-label, clinical trial that assessed T-DXd efficacy in patients with mBC. The DAISY trial complies with all relevant ethical regulations, overseen by the board/committee and institution that approved the study protocol. DAISY trial was approved by the French ethics committee (CPP), Île-de-France, on 5 September 2019 and the French health authorities (ANSM) on 8 July 2019. The first patient was enrolled on 4 November 2019 and the last one on 3 March 2021 in 15 study centers in France. The study design is reported in Extended Data Fig. 1. The first and last versions of the protocol are provided in the Supplementary Information. Patients with mBC were eligible if they had received at least one line of chemotherapy in the metastatic setting, had at least one non-bone metastatic lesion accessible to biopsy and had signed the informed consent for biopsies throughout the study. Both sexes were eligible based on self-report. Mandatory and optional biopsies are described in the protocol (Annex 1 and Annex 2). The biopsy at baseline could be skipped if a biopsy collected within 3 months before inclusion was available. Patients were assigned to three cohorts according to HER2 level expression determined by standard IHC, as previously reported³⁷, on samples obtained at baseline biopsy. Patients with HER2-overexpressing mBC had to be pretreated with taxane and to be resistant to trastuzumab and T-DM1. Patients with HER2-low or HER2 IHC 0 tumors had to be pretreated with anthracyclines and taxanes. Patients with tumor-expressing hormone receptors had to be resistant to endocrine therapy and CDK4/6 inhibitors. No safety monitoring board was involved in the study.

Treatments and follow-up

After signature of the informed consent, patients were treated with T-DXd intravenously 5.4 mg kg⁻¹ every 3 weeks until disease progression or unacceptable toxicity, as defined by the investigator. Recommendations for dose reductions are described in the V1 of the protocol (Annex 1). Treatment efficacy was monitored by a computed tomography (CT) scan every 6 weeks during the initial 12 months and every 12 weeks thereafter. The CT scan was repeated at least 4 weeks after assessment of a partial response or a complete response. Response Evaluation Criteria in Solid Tumors (RECIST) version 1.1 were used to determine response and progression³⁸. Toxicity data were collected at each visit and classified according to the National Cancer Institute Common Terminology Criteria for Adverse Events (CTCAE) version 5.0.

IHC

For cohort allocation, HER2 status was determined by a GEPFICS trained pathologist³⁹ on the biopsy performed at baseline (Extended Data Fig. 2). Estrogen and progesterone receptor status were determined locally, with a cutoff for positivity set at 10% of tumor cells. HER2 status was defined according to the last version of the American Society of Clinical Oncology (ASCO)/College of American Pathologists (CAP) guidelines³⁷. ‘Ultra-low’ HER2 category was defined as cases showing a faint to weak incomplete membrane staining in less than 10% of tumor cells (that is, less than 1+, classified in the IHC 0 category following the ASCO/CAP guidelines³⁷). HER2 staining on biopsies at progression was performed centrally at Gustave Roussy using the 4B5 pre-diluted kit (VENTANA pathway HER2, clone: 4B5, Roche Diagnostics), according to the manufacturer’s protocol. Twenty-five pairs of tumor biopsies obtained at baseline and progression were assessed (Extended Data Fig. 7).

Regarding T-DXd distribution during treatment, 10 paired baseline and on-treatment tumor biopsies were initially selected. Three pairs were not analyzed owing to the lack of tumor cells. Seven pairs of tumor biopsies, four from cohort 2 and three from cohort 3 (days 2–4 cycle 1, $n = 5$; day 7 cycle 2, $n = 1$; day 1 cycle 5, $n = 1$), were stained. Staining was done for HER2 with VENTANA anti-HER2/neu (4B5) rabbit monoclonal primary antibody (VENTANA pathway HER2, clone: 4B5, Roche Diagnostics) according to the manufacturer’s instructions,

and, when necessary, the enhanced HER2 protocol was employed to detect low level of HER2 expression. For the enhanced HER2 protocol, OptiView DAB IHC Detection Kit (Roche Diagnostics) was used instead of ultraView Universal DAB Detection Kit (Roche Diagnostics). HER2 was defined according to the last version of the ASCO/CAP guidelines³⁷. Tissue sections were stained for DXd-IgG using primary antibody against DXd (antiXAFG5737-1A3-ocChimera, Daiichi Sankyo) with Leica BOND RX automated slide stainer (Leica Biosystems). Rabbit isotype control antibody (PA0777, Leica Biosystems) was used as negative reagent control. Anti-DXd was raised against a part of DXd and can recognize free DXd. However, in formalin-fixed, paraffin-embedded (FFPE) samples, the intracellular, cleaved, free DXd is expected to be washed out during sample preparation and IHC procedure because DXd does not contain formaldehyde-sensitive group (that is, -NH₂). The IHC procedure washed away the free DXd, which resulted in the DXd-IgG primarily detecting T-DXd. The distribution and the percentage of DXd-IgG-positive cells in total tumor cells was evaluated. In addition to the seven pre-/on-treatment biopsies, DXd staining was also performed in six paired tissue biopsies obtained at baseline and resistance from cohort 1 (Extended Data Fig. 7).

Multiplex immunofluorescence was performed with the Ultivue kit containing the Immuno8 FixVUE panel composed of eight pre-diluted antibodies (twice four barcoded markers) + DAPI ready to use. The antibodies were directed against CD3 (clone BC33), CD4 (clone SP35), CD8 (clone C8/144B), CD68 (clone KP-1), FoxP3 (clone 236A/E7), PD-1 (clone CAL20), PD-L1 (clone 73-10) and PanCK/SOX10 (clone AE1/AE3/BC34). Thirty-one paired FFPE tumor biopsies obtained at baseline and on days 22–43 after cycle 1 were stained (18 cohort 1, 10 cohort 2, three cohort 3; Extended Data Fig. 7). After each detection cycle and hematoxylin, eosin and saffron (HES) staining, slides were imaged using the Akoya Biosciences PhenolImager HT. For each sample, the three whole slide images (WSIs) were stacked in one by Ultivue. The resulting stacked WSIs were analyzed in QuPath 0.3.2 (ref. 40) software. Regions of interest (ROIs) were manually delineated by a pathologist (M.L.T.). Inside these regions, tissue was automatically detected using a trained classifier. The number of stained cells per square millimeter of analyzed tissue was determined for each marker. In addition, the distance between each cell and the nearest CK⁺ cell was computed.

HER2 spatial distribution analysis by machine learning

Slides stained for HER2 expression collected at baseline from cohort 1 were digitalized and analyzed through an unsupervised clustering algorithm ($n = 61$; seven slides were not exploitable or could not be digitalized with the appropriate scanner; Extended Data Fig. 5). Unsupervised clustering algorithms aimed to identify groups of patches sharing similar features across the slides (clusters). A pathologist (I.J.G.) annotated the ROIs in the slides to discard biopsies without tumor tissue and tissue regions outside viable tumor. We contoured each tissue within these annotated areas using morphological operations. We downsampled the slides by a factor of 8 in each dimension to reduce image size and applied a grayscale conversion. We then subtracted the local average over a window size of 30×30 from each pixel to retrieve an image near-zero mean and computed the law texture energy measures. Finally, we applied a binary threshold on the spot texture map (above 20) with a flood fill algorithm to discard eventual artifacts (blurry regions and ink stains) and extract final tissue contours. We isolated main tissues by enforcing a minimum area criterion (above 1,500) to remove noisy elements introduced by the pre-processing. We chose a patch size of 64×64 , without overlap, to carry the analysis at the level of a few cells and removed black and white patches by removing patches with over 70% of RGB values below 2 and 80% of RGB values above 250. Following Lu et al.⁴¹, we extracted 1,024 visual appearance descriptors by applying a ResNet50 model truncated after the third residual block and pre-trained on ImageNet.

We applied Mini-Batch K-means⁴² to extract clusters across all the slides from the patch descriptors, normalized by their mean and s.d. To determine the optimal number of clusters, we computed the Davies–Bouldin index within a range around nine clusters (from seven to 12)⁴³. A segmentation into eight clusters minimized the score on this interval (Extended Data Fig. 6), and so we selected this value. For each slide i containing N_i patches, we computed the cluster assignment of each patch $L_{n_i} \in \{0 \dots 7\}$ using the trained clustering algorithm. We retrieved a vector of eight features $V_i \in [0, 1]^8$ for each slide by counting the proportion of patches for each label:

$$V_i[k] = \frac{1}{N_i} \sum_{n_i=1}^{N_i} 1_{\{L_{n_i}=k\}} \text{ for } k \in \{0 \dots 7\}$$

The clusters were further analyzed on the ground of nuclei statistics toward the design of interpretable markers using an unsupervised nuclei segmentation algorithm⁴⁴. To adapt the heterogeneous staining condition of DAISY slides, we added several modifications to the original methodology. We added color jittering to the consistency loss as well as instance normalization instead of batch normalization while retraining on the same HER2 public data to help to improve the model generalization. Then, we implemented a new stain deconvolution method better tailored to IHC imaging⁴⁵. Lastly, we selected the best model to predict nuclei masks for DAISY data under the guidance of an expert pathologist selecting the checkpoint to be used. The nuclei were then segmented on 256×256 -pixel (px) overlapping patches, with 50% overlap obtained with the same pre-processing described for the clustering. To interpret clustering decision, we computed several features based on nuclei properties and density in the patches of size 64×64 used to compute the clustering (Supplementary Fig. 5). Nuclei with their centroids within 20 px (that is, $6.5 \mu\text{m}$) of an already segmented nucleus were discarded. We also implemented a test time augmentation scheme⁴⁶ to correct the segmentation on low-contrast patches by dividing the slides into two groups, depending on the correction needed, and took the minimum between the predictions from increased contrast versions from the original image. We finally exported the segmentation to QuPath 0.4.0 (ref. 40) to extract shape and intensity features (such as area, perimeter, circularity and DAB intensity within $30\text{-}\mu\text{m}$ diameter circular tile) and removed the remaining artifacts by enforcing a threshold on the perimeter and circularity of the predicted nuclei. We ultimately averaged the resulting values over the nuclei detected in the patches of size 64×64 used to compute the clustering—that is, whose centroid is located the patch—to get one value by marker for each patch and counted the number of nuclei detected in each patch to construct a cell density measure.

The association between the confirmed objective response and clusters was assessed through statistical analysis based on each cluster's relative percentage in each slide. We used a Mann–Whitney U -test to assess if there was a statistically significant difference between the percentage of each cluster and the confirmed response to T-DXd. All P values were adjusted for multiple hypothesis testing using the Benjamini–Hochberg method. Finally, two pathologists (I.J.G. and M.L.T.) reviewed the cell phenotype in cluster 6. The same protocol followed for cohort 1 was used to train a new model in cohort 2 ($n = 65$; Extended Data Fig. 5 and Supplementary Fig. 6). ROIs were not annotated in HER2 pathology slides from cohort 2.

RT-PCR

Tumor samples obtained at baseline from cohort 3 (HER2 IHC 0) were qualified for RT-PCR if the sample contained $\geq 30\%$ tumor cells ($n = 24$). Then, $1 \mu\text{g}$ of RNA was reversed into cDNA with SuperScript Vilo cDNA Synthesis Kit (Thermo Fisher Scientific). Quantitative PCR was performed with TaqMan Fast Advanced Master Mix using TaqMan Gene Expression Assays, Hs01111580 (HER2), Hs00197427 (*ACTB*) and HS99999901 (*18S*), as recommended by the supplier (Thermo Fisher

Scientific). *18S* and *ACTB* were used as internal references to normalize input cDNA. The comparative threshold (ΔC_t) method was used to quantify *ERBB2* expression. The median of *ERBB2* relative expression was 30. The confirmed ORRs were assessed according to *ERBB2* expression levels ($<$ or $>$ median expression). Association with efficacy was done with the confirmed objective response.

Genomic analyses

The tumor samples were qualified for WES if the sample contained $\geq 30\%$ tumor cells. In total, 89 frozen tumor biopsies at baseline (38 cohort 1, 37 cohort 2, 14 cohort 3) and 21 (5 cohort 1, 11 cohort 2, 5 cohort 3) at resistance were analyzed. Eighty-four blood samples were used as germline control. Genomic DNA was isolated from biopsy and blood of patients using the QIAamp DNA Mini Kit and DNeasy Blood and Tissue Kit (Qiagen), respectively, according to the manufacturer's guidelines. DNA concentration was measured using Qubit™ dsDNA Broad Range Assay (Invitrogen). A quantity of $30\text{--}100 \text{ ng}$ of DNA was used for preparing the WES libraries. For the WES, the DNA was sheared with the Covaris E220 system (LGC Genomics/KBioscience). SureSelect Low Input Target Enrichment was used. In brief, DNA fragments were end-repaired, extended with an 'A' base on the 3' end, ligated with paired-end adaptors with the Bravo Platform (Agilent Technologies) and amplified to generate libraries (10 cycles). Hybridization-based exome enrichment was performed using the Agilent SureSelect Low Input Clinical Research Exome V2 target enrichment system (Agilent Technologies). The final libraries were indexed, pooled and sequenced using the onboard cluster method, as paired-end sequencing ($2 \times 100\text{-bp}$ reads) on an Illumina NovaSeq 6000 sequencer at Gustave Roussy.

Statistical analyses of association with efficacy were done with the confirmed objective response.

Bioinformatic analyses

Point mutations, small indels and CNAs were detected using an end-to-end pipeline described previously⁴⁷. In brief, paired-end reads were controlled (FastQC version 0.11.8), trimmed (fastp version 0.20) and aligned to the reference human genome GRCh37 (BWA-MEM version 0.7). Aligned reads were processed following the best practices of GATK bundle version 4.1.8.1. Processed reads were then used as input to mutation-calling and CNA-calling algorithms. As advised in GATK guidelines, we used a panel-of-normal to remove artifactual or false-positive mutations recurrently found in normal blood samples from patients with cancer treated at Gustave Roussy. Point mutations and small indels were called using Mutect2 (ref. 48) and the panel-of-normal. All putative variants identified by Mutect2 were first filtered to account for possible sample contamination and read orientation artifacts. Additional threshold-based and rule-based filtering was applied to the read coverage, genomic position and variant allele frequency (VAF). Specific rules were applied to tumor samples from patients with WES at baseline and progression (11 patients). More particularly, for each baseline (and progression, respectively) sample, SAMtools version 1.9 mpileup⁴⁹ was run on the positions where Mutect2 identified and retained mutations in the corresponding progression (and baseline, respectively) sample to rule out incorrect claims of mutation acquisition or loss caused by conservative filtering or non-detection by Mutect2. If a mutation detected by Mutect2 in a sample at a given timepoint was also seen in the sample from the other timepoint with sufficiently many reads supporting the alternative allele (at least one read if coverage < 100 , two reads if $100 \leq \text{coverage} < 500$ and three reads if coverage > 500), the mutation was also called in the latter sample. Additionally, in patients without a matched blood sample, any mutation identified as germline at any of the two timepoints was discarded from both samples. After all the filtering, 20,469 somatic point mutations and small indels were considered in the analysis of the 110 WES samples (89 at baseline, 21 at resistance; Supplementary Fig. 7).

CNAs, tumor purity and average tumor ploidy were identified with the FACETS R package version 0.5.14 (ref. 50) run with parameters $cval_pre = 25$ and $cval_pro = 500$. To mitigate the effect of segmentation errors, only gene CNAs arising from segments spanning fewer than 10 Mb were considered in downstream analyses. Additionally, in an effort to increase the sensitivity of CNA calling on driver genes, a second run of FACETS with parameters $cval_pre = 25$ and $cval_pro = 150$ was performed and used to replace the copy number estimations on driver genes only if the second-run segment was smaller than 3 Mb in size or three times smaller than the first-run segment. Each CNA was classified into one of six categories⁴⁷, and only high-level focal amplifications (medium-level also considered for oncogenes) or homozygous focal deletions were considered. Oncogenic events were identified by intersecting point mutations, small indels, gene amplifications and gene deletions with the OncoKB database (December 2022 release, <https://github.com/oncokb/oncokb-annotator>)⁵¹.

Patient and sample attributes for the TCGA cohort were downloaded from the GDC data portal ([gdc-tcga-phs000178-controlled](https://gdc.cancer.gov/about-data/publications/pancanatlas)) using the R package GenomicDataCommons version 1.18.0 and from the supplementary tables publicly available on the PanCanAtlas page (<https://gdc.cancer.gov/about-data/publications/pancanatlas>). Only patients included in the BRCA study of TCGA and for which we found no reason for exclusion were considered (Supplementary Fig. 8). Point mutations and small indels for TCGA samples were downloaded with permission from the file `mc3.v.0.2.8.CONTROLLED.maf.gz` (<https://gdc.cancer.gov/about-data/publications/mc3-2017>)⁵² and filtered as follows. All point mutations seen by at least two callers among the five used by MC3 (ref. 52) and all small indels seen by INDELOCATOR or VARSCANI were selected. These putative variants were then filtered using the same threshold-based and rule-based filtering as used on DAISY samples. This filtering procedure was carefully determined to maximize the alignment between our internal pipeline and the MC3 pipeline⁴⁷. WES BAM files for TCGA BRCA patients were downloaded with permission and processed with FACETS using the same pipeline as used for DAISY samples.

In vitro experiments

MCF-7 and SK-BR-3 cells were purchased from the German Collection of Microorganisms and Cell Cultures. MCF-7 cells were grown in DMEM (Gibco) supplemented with 1% GlutaMAX (Gibco) and SK-BR-3 in McCoy's 5A medium (Gibco) in standard incubation conditions at 37 °C with 5% CO₂. Both media were supplemented with 10% FBS, penicillin (100 U ml⁻¹) and streptomycin (100 µg ml⁻¹) and cells. All cell lines were kept as mycoplasma-free. Cells were seeded at 5×10^3 cells per well in a 96-well plate. Twenty-four hours later, cells were transfected with the siRNAs targeting *SLX4* gene (ON-TARGETplus siRNA, SMARTpool, Dharmacon) or Non-targeting Control Pool (Dharmacon) according to the manufacturer's instructions. To evaluate cell viability, DXd was added 48 h after siRNA transfection with eight-point dose–response titrations in triplicate (0.1–1,000 nM) for 5 days. Cell viability was examined using the CellTiter-Glo Luminescent Cell Viability Assay (Promega) using a VICTOR Nivo multimode plate reader (PerkinElmer). Survival at each drug concentration was calculated as a percentage relative to the corresponding untreated control. To assess *SLX4* expression, total RNAs were extracted using RNeasy Mini Kit (Qiagen) and reversed into cDNA with Maxima Reverse Transcriptase (Thermo Fisher Scientific). Quantitative PCR was performed with Master Mix PCR Power SYBR Green (Life Technologies) using CFX96 Real Time System (Bio-Rad). The specific primers for *SLX4* used in this study were 5'-GTGAAGGTCGGAGTCAACG-3' and 5'-GGTGAAGACGCCAGTGGACTC-3'. GAPDH was used as an internal reference to normalize input cDNA. The ΔC_t method was used. Data were expressed as mean \pm s.e.m. for $n = 3$. For viability assay, significance was analyzed by Welch's *t*-test (two-tailed). Statistical analysis was performed using GraphPad Prism 9 (GraphPad Software). *P* values less than 0.05 were considered statistically significant.

Statistical analyses

The primary endpoint was the confirmed ORR evaluated by investigator assessment using RECIST 1.1. The secondary endpoints included duration of response, PFS, OS and clinical benefit rate evaluated on the FAS and per cohort. Safety was evaluated on the safety population and per cohort. The required number of assessable patients for cohort 1 ($n = 67$) and cohort 2 ($n = 40$) was determined using the A'Hern design with the following hypothesis: cohort 1 ($p_0 = 30\%$; $p_1 = 45\%$; $\alpha = 5\%$; power = 80%) and cohort 2 ($p_0 = 20\%$; $p_1 = 40\%$; $\alpha = 5\%$; power = 85%). The regimen would be declared promising in cohort 1 if 27 patients present a confirmed objective response among 67 and in cohort 2 if 13 confirmed objective responses were observed among 40. The required number of assessable patients for cohort 3 ($n = 40$) was designed using an optimal two-stage design⁵³ ($\alpha = 5\%$, power = 85%) with non-progression at 3 months as short-term endpoint ($p_{20} = 30\%$, $p_{21} = 50\%$) and confirmed objective response as primary endpoint ($p_{10} = 20\%$, $p_{11} = 40\%$). A stop for non-promising activity was planned to be declared if four patients or fewer among the first 16 present non-progressive disease at 3 months. At final analysis of cohort 3, the regimen would be defined as promising if 13 patients or more present a confirmed objective response among 40. In cohort 3, recruitment was stopped after 40 patients (37 assessable for activity) because of slow recruitment. For each cohort, it was assumed a rate of 10% non-evaluable patients, and sample size was increased: cohort 1: $n = 74$, cohort 2: $n = 44$, cohort 3: $n = 44$. Full details are provided in the Statistical Analysis Plan.

The primary endpoint was reported for each cohort, and comparisons were considered exploratory. Comparison between cohorts was performed using the chi-square test or Fisher's exact test for qualitative variables and the Kruskal–Wallis test for continuous variables; and multivariable analysis was performed using logistic regression model adjusted for hormone receptor status of primary tumor (hormone receptor-positive versus hormone receptor-negative), time from initial diagnosis to metastatic disease (0–3 months versus >3 months), time from diagnosis of metastatic disease to inclusion (0–24 months versus 24–60 months versus >60 months), number of metastatic sites (<3 versus ≥ 3 sites), presence of liver metastases (yes versus no) and ECOG performance status (0 versus 1) at inclusion. ORs were estimated with corresponding 95% CI. The best tumor shrinkage of target lesions was plotted on a waterfall plot and compared between cohorts using the Kruskal–Wallis test. Time to event endpoints (PFS and duration of response) were estimated using the Kaplan–Meier method, and comparison between groups was performed using the log-rank test. Multivariable analysis was performed using Cox proportional hazards model adjusted for the same variables used for the confirmed objective response. HRs were estimated with corresponding 95% CI. In the exploratory objective of modulation of tumor microenvironment, comparisons of each biomarker at baseline and on-treatment were performed using the Wilcoxon matched-pairs signed-rank test. Cell distance analysis *P* values were adjusted for multiple hypothesis testing using the Benjamini–Hochberg method. All statistical tests were two-sided. Statistical analyses were performed using STATA software version 16 (StataCorp).

Reporting summary

Further information on research design is available in the Nature Portfolio Reporting Summary linked to this article.

Data availability

All data used in the present study are available within the manuscript and its Supplementary Information files.

Clinical data are available for access upon external requests. Applicants should contact the following email address 'mariafernanda.mosele@gustaveroussy.fr' to request access to clinical data. The request will be discussed internally in the joint steering committee of the study. The decision will be communicated within 1 month from the

request. Applicants must complete specific documents to be granted a user license.

Whole-exome sequencing data generated in this study have been deposited to the European Genome-phenome Archive (EGA) under accession number [EGAD00001011110](https://ega-archive.org/studies/EGAD00001011110). Refer to the forms and README file from https://github.com/gustaveroussy/DAISY_Public/tree/master/data for instructions on how to access the data. Other data that support the findings of this study are available from the corresponding author upon reasonable request.

Databases used in the study include gnomAD (<https://gnomad.broad-institute.org>), OncoKB Precision Oncology Knowledge Base (<https://www.oncokb.org>), Clinical Interpretation of Variants in Cancer (<https://civicdb.org>) and dbNSFP version 4.1.a (<https://sites.google.com/site/jpopgen/dbNSFP>).

Code availability

The source code to reproduce the analyses presented in this paper is available at https://github.com/gustaveroussy/DAISY_Public.

References

37. Wolff, A. C. et al. Human epidermal growth factor receptor 2 testing in breast cancer: American Society of Clinical Oncology/ College of American Pathologists clinical practice guideline focused update. *J. Clin. Oncol.* **36**, 2105–2122 (2018).
38. Schwartz, L. H. et al. RECIST 1.1—update and clarification: from the RECIST committee. *Eur. J. Cancer* **62**, 132–137 (2016).
39. Franchet, C. et al. [2021 update of the GEPICS' recommendations for HER2 status assessment in invasive breast cancer in France]. *Ann. Pathol.* **41**, 507–520 (2021).
40. Bankhead, P. et al. QuPath: open source software for digital pathology image analysis. *Sci. Rep.* **7**, 168–178 (2017).
41. Lu, M. Y. et al. Data-efficient and weakly supervised computational pathology on whole-slide images. *Nat. Biomed. Eng.* **5**, 555–570 (2021).
42. Pedregosa, F. et al. Scikit-learn: machine Learning in Python. *J. Mach. Learn. Res.* **12**, 2825–2830 (2011).
43. Kalra, S. et al. Yottixel—an image search engine for large archives of histopathology whole slide images. *Med. Image Anal.* **65**, 101757 (2020).
44. Le Bescond, L. et al. Unsupervised nuclei segmentation using spatial organization priors. In *Medical Image Computing and Computer Assisted Intervention—MICCAI 2022* (eds. Wang, L., Dou, Q., Fletcher, P. T., Speidel, S. & Li, S.) 325–335 (Springer Nature Switzerland, 2022).
45. Geijs, D. J., Intezar, M., van der Laak, J. A. W. M. & Litjens, G. J. S. Automatic color unmixing of IHC stained whole slide images. In *Proceedings Vol. 10581*, 165–171. <https://doi.org/10.1117/12.2293734> (2018).
46. Scalbert, M., Vakalopoulou, M. & Couzinié-Devry, F. Test-time image-to-image translation ensembling improves out-of-distribution generalization in histopathology. In *Medical Image Computing and Computer Assisted Intervention—MICCAI 2022* (eds. Wang, L., Dou, Q., Fletcher, P. T., Speidel, S. & Li, S.) 120–129 (Springer Nature Switzerland, 2022).
47. Pradat, Y. et al. Integrative pan-cancer genomic and transcriptomic analyses of refractory metastatic cancer. *Cancer Discov.* **13**, 1116–1143 (2023).
48. Cibulskis, K. et al. Sensitive detection of somatic point mutations in impure and heterogeneous cancer samples. *Nat. Biotechnol.* **31**, 213–219 (2013).
49. Li, H. et al. The Sequence Alignment/Map format and SAMtools. *Bioinformatics* **25**, 2078–2079 (2009).
50. Shen, R. & Seshan, V. E. FACETS: allele-specific copy number and clonal heterogeneity analysis tool for high-throughput DNA sequencing. *Nucleic Acids Res.* **44**, e131 (2016).
51. Chakravarty, D. et al. OncoKB: a precision oncology knowledge base. *JCO Precis. Oncol.* **2017**, PO.17.00011 (2017).
52. Ellrott, K. et al. Scalable open science approach for mutation calling of tumor exomes using multiple genomic pipelines. *Cell Syst.* **6**, 271–281 (2018).
53. Kunz, C. U., Wason, J. M. & Kieser, M. Two-stage phase II oncology designs using short-term endpoints for early stopping. *Stat. Methods Med. Res.* **26**, 1671–1683 (2017).

Acknowledgements

We thank the patients and their families as well as the investigators and staff involved in the DAISY trial. This study was supported by Unicancer and PRECISION Medicine institute in oncology (PRISM), funded by the France 2030 program and the French National Research Agency (ANR) under grant number ANR-18-IBHU-000, and Daiichi Sankyo. We are grateful to Unicancer for promoting the clinical trial and especially to M.J. who was in charge of the DAISY clinical trial and all the members of their team that led the monitoring of the clinical data and sample shipment. We are also grateful to Daiichi Sankyo, which supported T-DXd supply to the study sites, to T. Shibutani, R. Yoshimoto and H. Takahashi for pathology experiment and support, and to N. Corcos for support with graphics.

Author contributions

F.M. coordinated the translational axis of the study and contributed to the writing. L.L.B. performed the artificial intelligence analyses. A.L. and T.F. ran all statistical analyses of the study. E.D., A.D., B.P., T.B., F.V. and C.L. were involved in recruitment, clinical care and data returns. Y.P., B.J. and M.D. performed bioinformatics analyses. V.M., N.S. and A.A. did the Multiplex IF analyses. I.J.G. participated in artificial intelligence analyses. H.T., S.C. and M.V. supervised the artificial intelligence analyses. D.T.N.T., N.D. and A.S. performed the genomic analyses of the trial. M.K. and T.K. performed the T-DXd distribution experiments at Japan. L.L. and P.S. did the RT-PCR analyses. M.J. and C.M. are the project managers of the DAISY trial and centralized the collected samples and data. V.B., P.L. and P.K. performed the in vitro experiments for SLX4. M.L.T. coordinated the translational axis, performed the immunochemistry analyses and participated in artificial intelligence and Multiplex IF. V.D. is the principal investigator of the study and was involved in recruitment, clinical care and data returns. F.A. designed the study, coordinated the translational axis, contributed to the writing and was involved in recruitment, clinical care and data returns. All authors approved the final manuscript and contributed to critical revisions of its intellectual content.

Competing interests

F.M. received consultant fees from Novartis and Pegascy. E.D. received personal fees and non-financial support from Novartis, Pfizer, AstraZeneca, Daiichi Sankyo, GlaxoSmithKline, Eli Lilly and Merck Sharp & Dohme. T.F. received consultant fees outside the submitted work and compensation to the institution from Cellectis, Roche and Eli Lilly. B.P. received fees as advisor/consultant from Pierre Fabre (self), Daiichi Sankyo (self), Merck Sharp & Dohme (institution), Seattle Genetics (institution), Eli Lilly (institution) and Novartis (institution); funding to institution for research support from Daiichi Sankyo and AstraZeneca; and travel expenses from AstraZeneca, Pfizer and Gilead. T.B. reports receiving grants and personal fees from Daiichi Sankyo, AstraZeneca, Pfizer and Seattle Genetics and personal fees from Novartis and Roche outside the submitted work. M.K. and T.K. are employees of Daiichi Sankyo RD Novare. M.L.T. received consultant fees as speaker and consultant from AstraZeneca and Daiichi Sankyo. V.D. received travel expenses from Roche, Novartis, Pfizer, Eli Lilly, AstraZeneca, Daiichi Sankyo, Seagen and Gilead; honoraria as consultant/advisor from Roche, Genentech, Novartis, Eli Lilly,

Pfizer, AstraZeneca, AbbVie, Merck Sharp & Dohme, Daiichi Sankyo, Seagen, Gilead, Eisai and Pierre Fabre Oncologie; and honoraria for symposia from Roche, Novartis, Pfizer, Eli Lilly, Astra Zeneca, Daiichi Sankyo, Seagen and Gilead. F.A. received research funding and served as speaker/advisor (compensated to the hospital) from Roche, AstraZeneca, Daiichi Sankyo, Pfizer, Novartis and Eli Lilly. The following authors have no disclosures: A.L., L.L.B., Y.P., A.D., F.V., C.L., N.S., A.A., D.T.N.T., I.J.G., H.T., S.C., M.V., N.D., A.S., L.L., P.S., J.B., M.D., M.J., C.M., V.B., P.L., P.K. and V.M.

Additional information

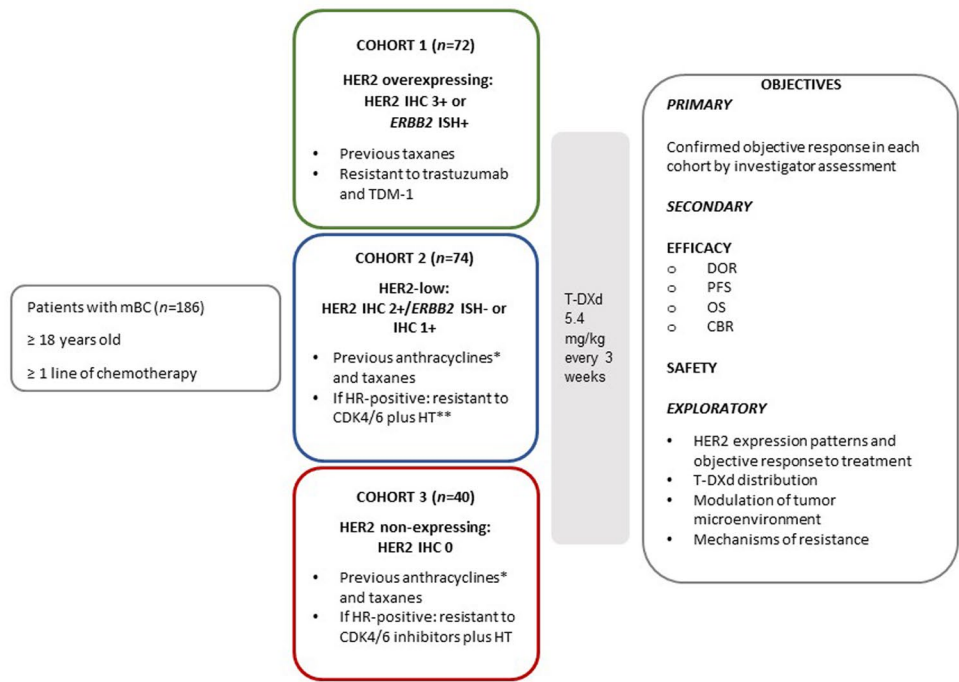
Extended data is available for this paper at <https://doi.org/10.1038/s41591-023-02478-2>.

Supplementary information The online version contains supplementary material available at <https://doi.org/10.1038/s41591-023-02478-2>.

Correspondence and requests for materials should be addressed to Fabrice André.

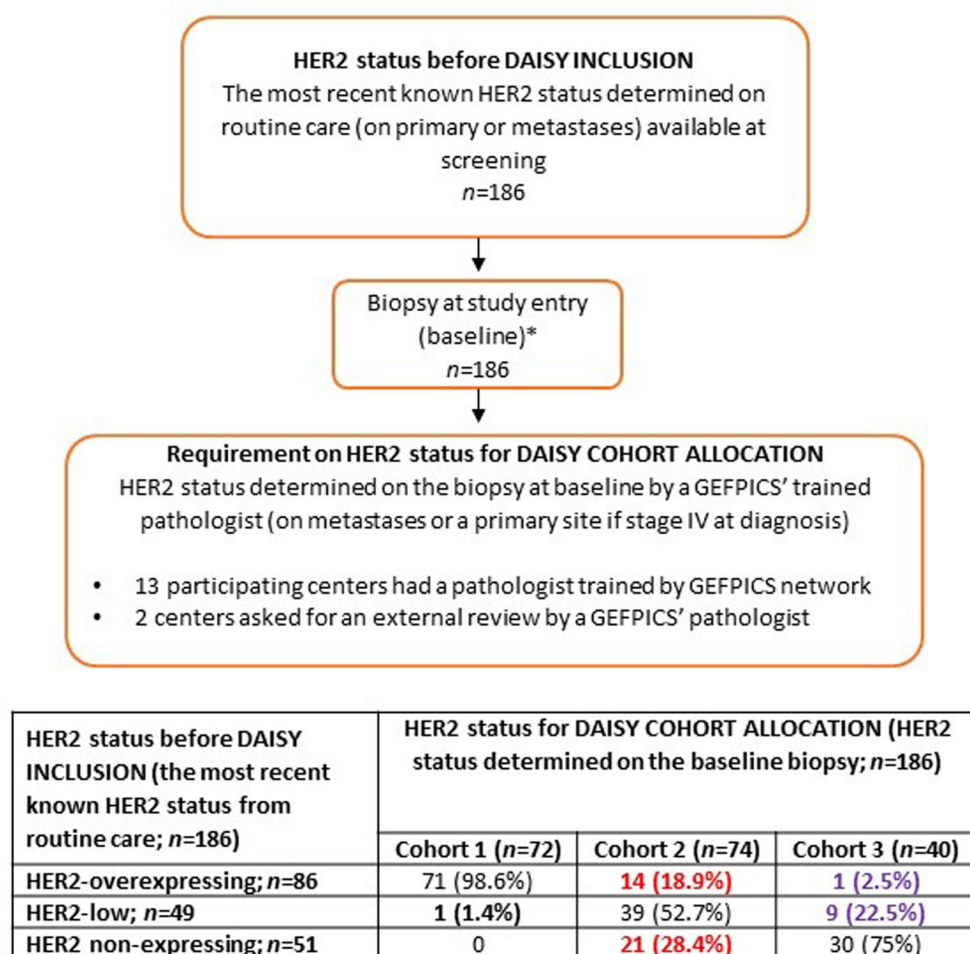
Peer review information *Nature Medicine* thanks Komal Jhaveri and the other, anonymous, reviewer(s) for their contribution to the peer review of this work. Primary handling editor: Saheli Sadanand, in collaboration with the *Nature Medicine* team.

Reprints and permissions information is available at www.nature.com/reprints.



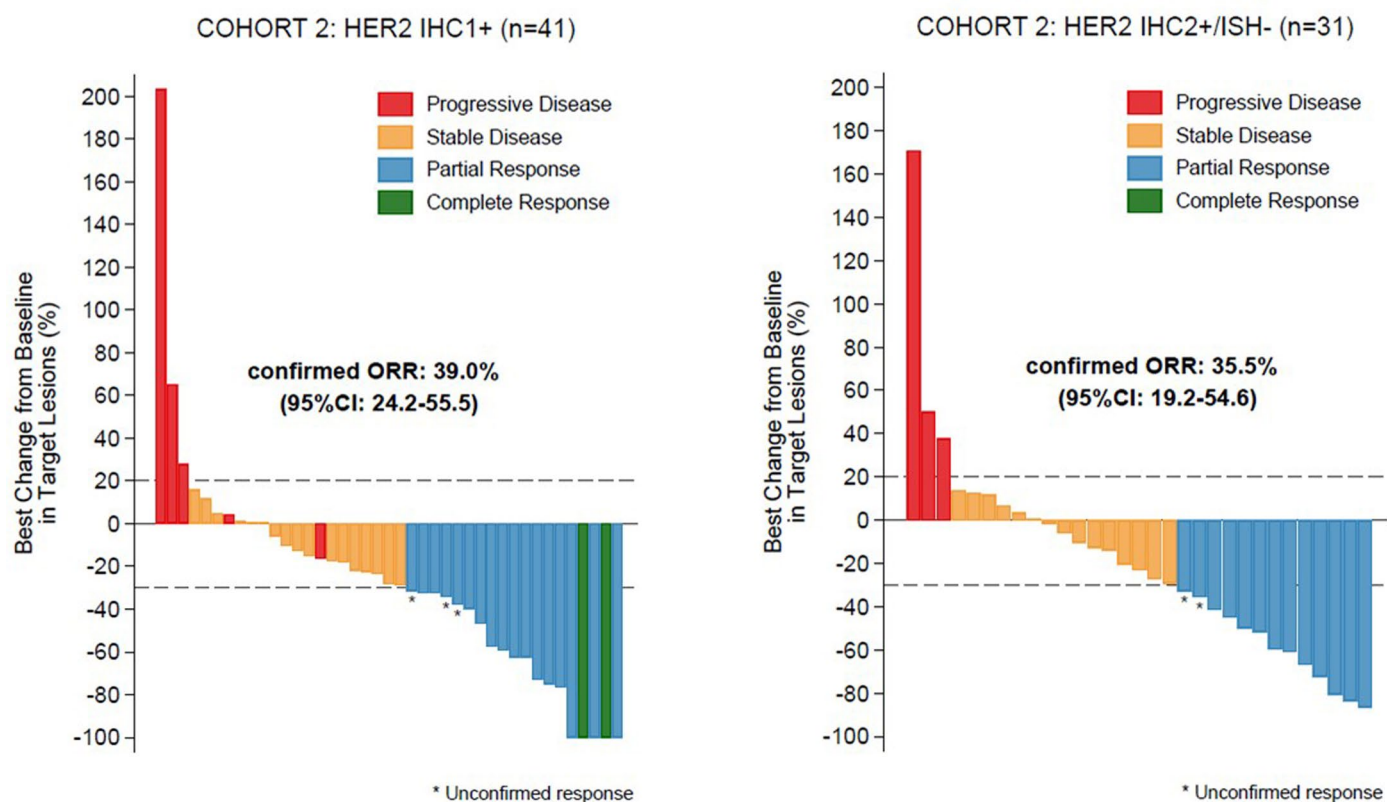
*A total of 5 patients from cohort 2 and 3 did not receive prior anthracyclines, either because anthracyclines were contraindicated, the primary tumor was HER2-overexpressing, or the patient had “de novo” metastatic HR-positive BC and the physician decided not to administer anthracyclines.
**Two patients from cohort 2 did not receive prior CDK4/6 inhibitors, 1 because had HER2-overexpressing BC before DAISY enrollment and the other one due to physician’s choice.
mBC: metastatic breast cancer; HER2: Human Epidermal growth factor Receptor 2; IHC: Immunohistochemistry; ISH: In situ hybridization; TDM-1: Ado trastuzumab emtansine; HR-positive: Hormone receptor positive; CDK4/6: Cyclin-dependent kinases 4 and 6; HT: Hormone therapy; PFS: Progression free survival; OS: Overall survival; DOR: Duration of response; CBR: Clinical benefit rate; T-DXd: Trastuzumab deruxitecan

Extended Data Fig. 1 | Study Design.

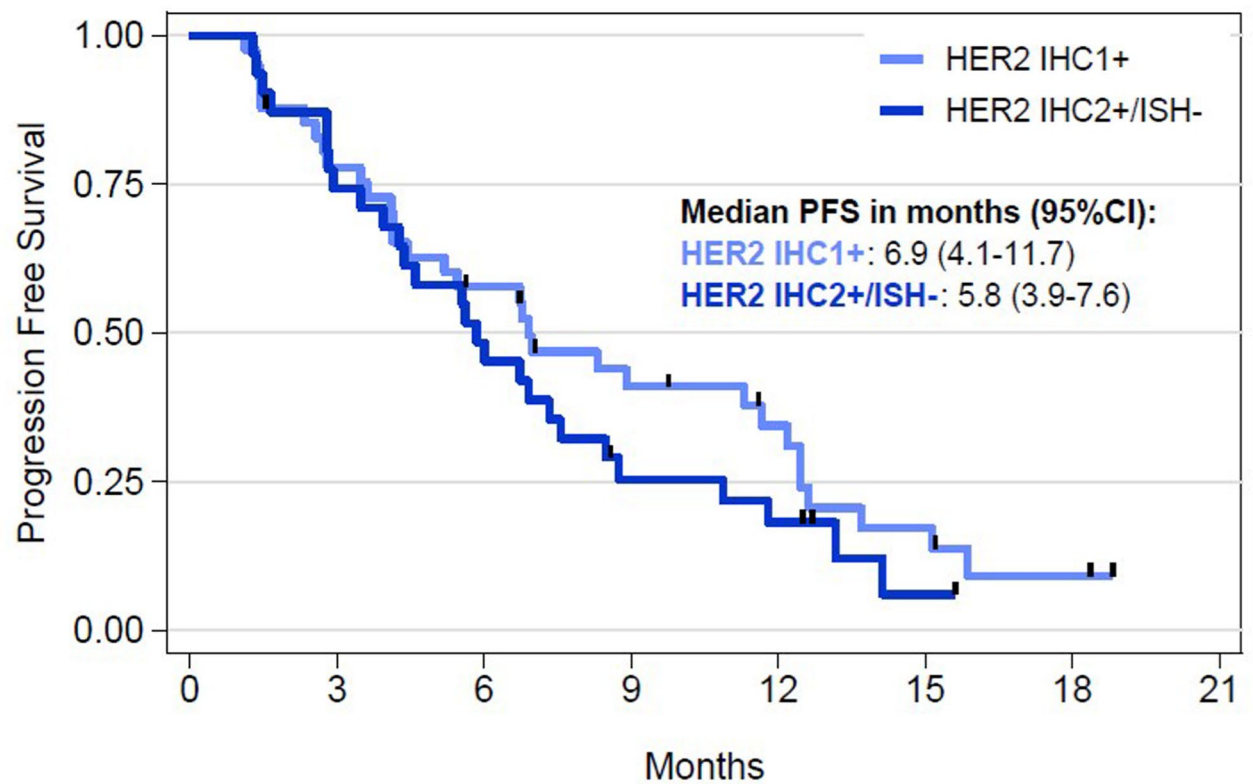


*An archived biopsy from a metastasis or a primary site, if stage IV at diagnosis, could be used for Cohort allocation provided that it was collected within 3 months prior enrolment.

Extended Data Fig. 2 | Determination of HER2 status by standard immunohistochemistry before DAISY inclusion and for cohort allocation.

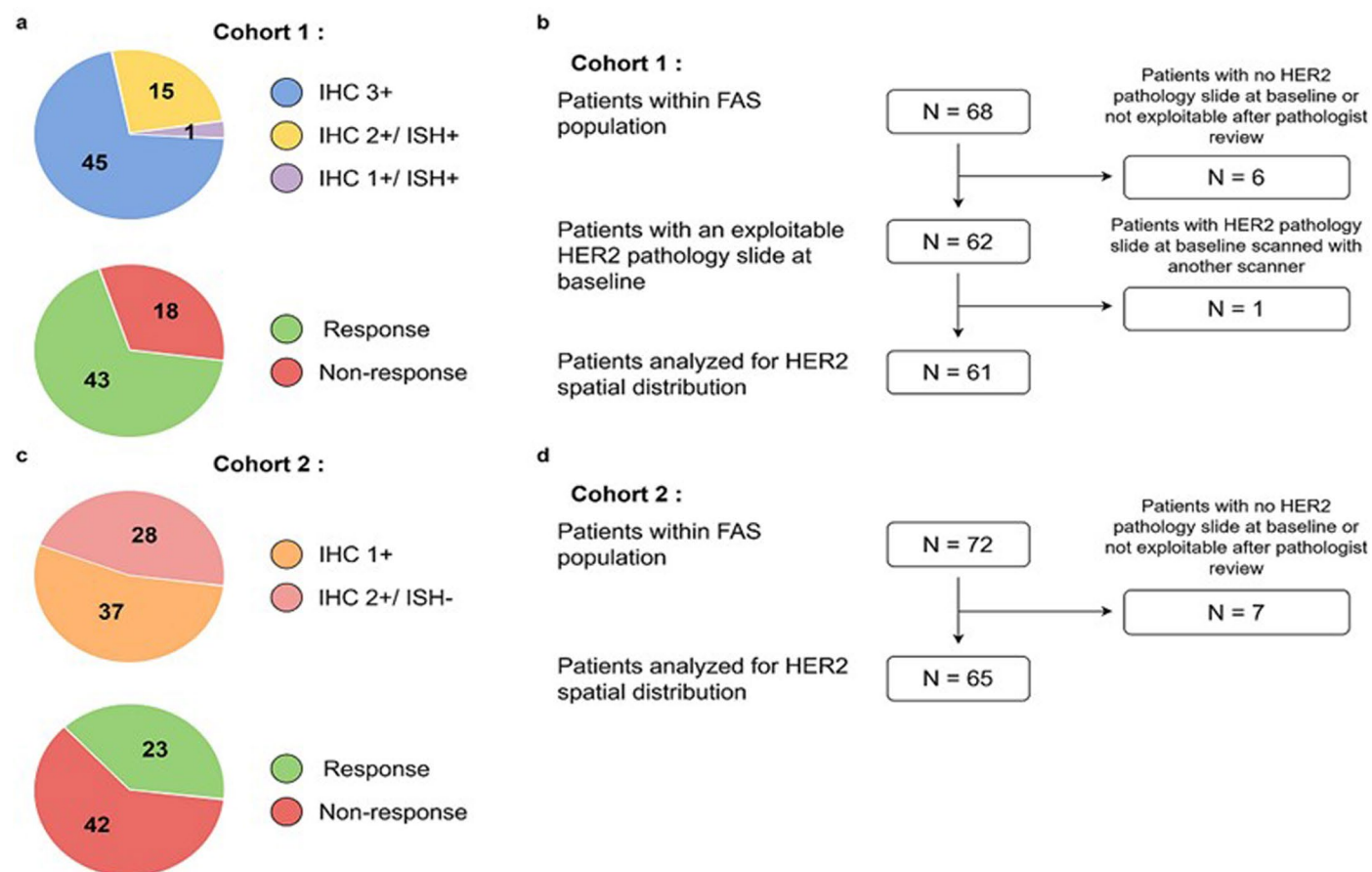


Extended Data Fig. 3 | Waterfall plot of the best change from baseline in target lesions according to the best objective response of patients from cohort 2 in FAS population ($n = 72$) according to HER2 status. On the left, patients with HER2 IHC 1+ ($n = 41$) and on the right patients with HER2 IHC 2+ /*ERBB2* ISH- ($n = 31$) treated with T-DXd.

COHORT 2: HER2-low ($n=72$)

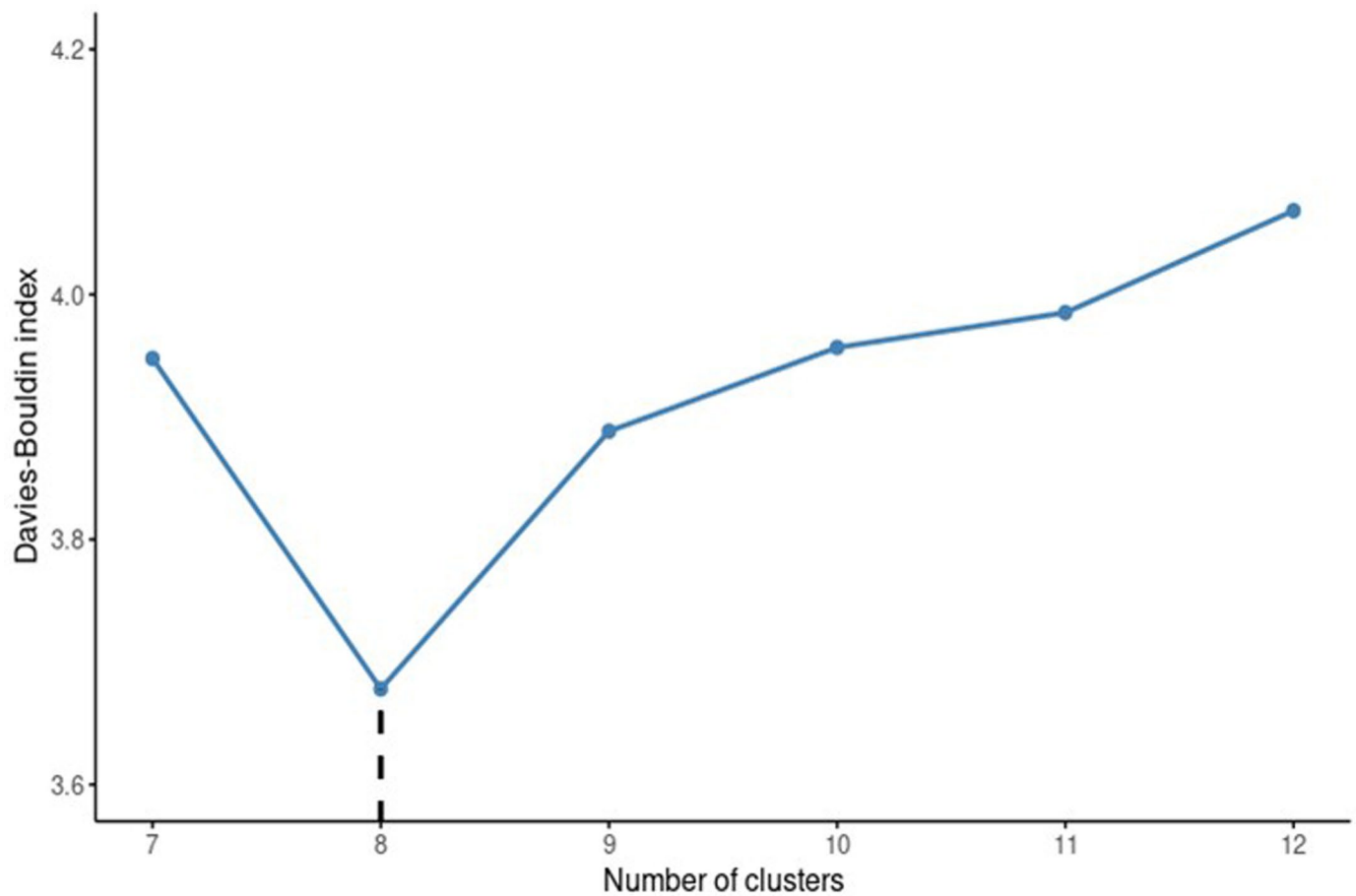
HER2 IHC1+	41	31	22	14	10	5	2	0
HER2 IHC2+/ISH-	31	23	15	7	5	1	0	0

Extended Data Fig. 4 | Kaplan-Meier plot of PFS in the FAS population from cohort 2 ($n = 72$) according to HER2 status. The median PFS was 6.9 months (95% CI 4.1-11.7) in patients with IHC 1+ ($n = 41$) and 5.8 months (95% CI 3.9-7.6) in patients with IHC 2+ /*ERBB2* ISH- mBC ($n = 31$).

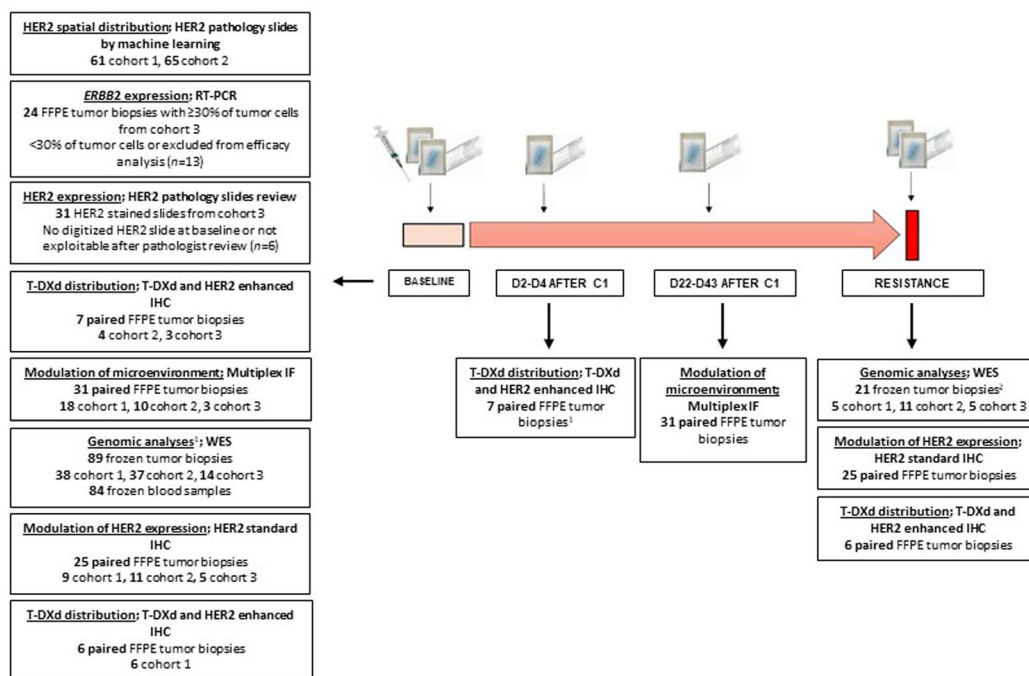


Extended Data Fig. 5 | Dataset description for HER2 expression spatial analysis. **a.** Distribution of HER2 IHC score and confirmed objective response in the dataset in cohort 1 (HER2-overexpressing). The numbers represent the number of patients analyzed ($n = 61$). **b.** Description of the patient set considered

for HER2 spatial distribution analysis in cohort 1. **c.** Distribution of HER2 IHC score and confirmed objective response in the dataset in cohort 2 (HER2-low). The numbers represent the number of patients analyzed ($n = 65$). **d.** Description of the patient set considered for HER2 spatial distribution analysis in cohort 2.



Extended Data Fig. 6 | Identifying an optimal number of clusters in cohort 1. The Davies-Bouldin index was computed from Mini-Batch K-Means clustering using a number of clusters ranging from 7 to 12. This index represents how the clusters are similar to each other, with a lower value pointing toward a better segmentation. Minimum is highlighted on the graph at 8 clusters.

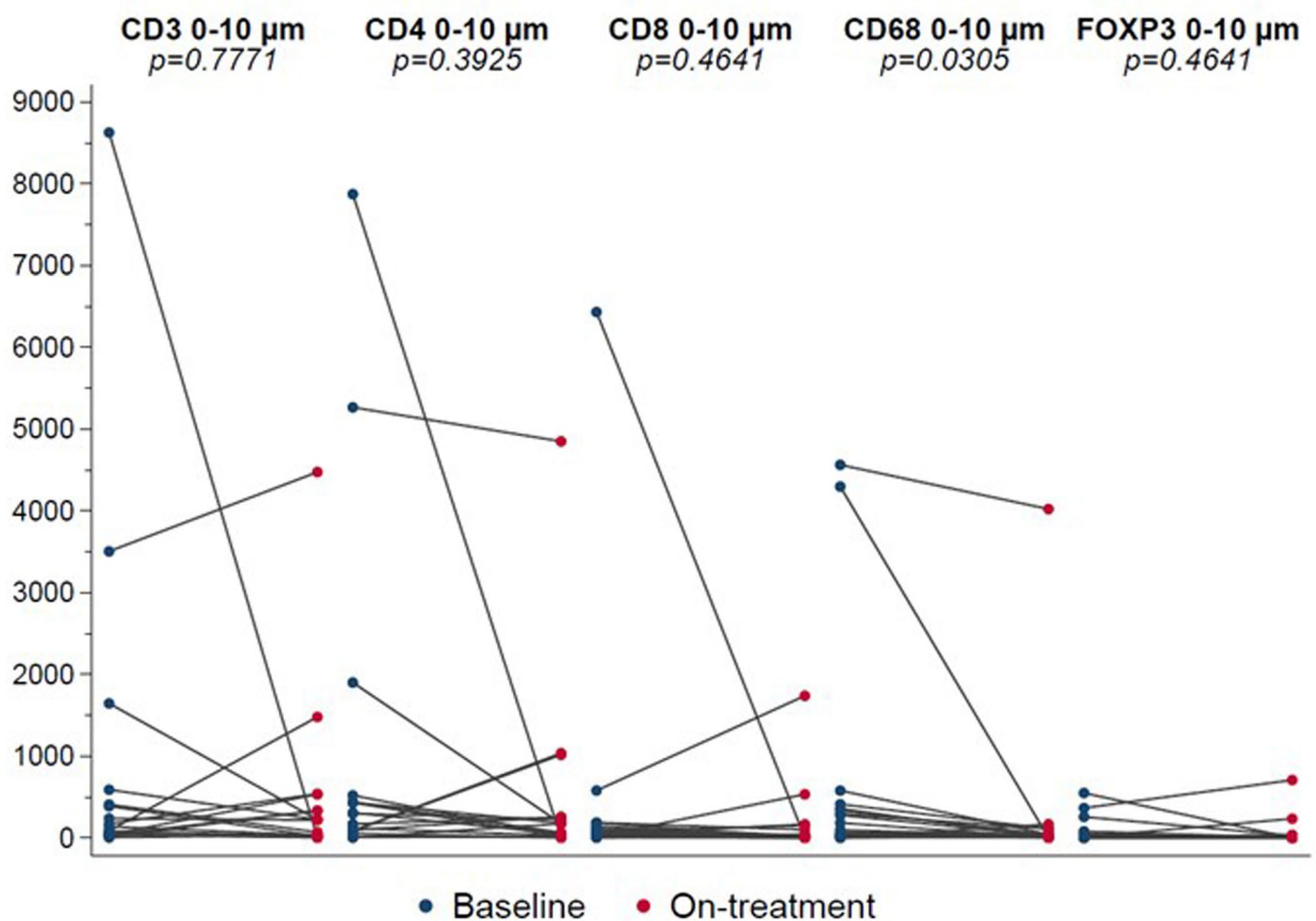


¹For T-DXd distribution assessment during treatment, tumor biopsies were performed on D2-D4 after C1 (n=5), on D7 after C2 (n=1) and on D1 of C5 after infusion of T-DXd (n=1).

²11 biopsies at resistance were matched with baseline biopsy

HER2: Human Epidermal growth factor Receptor 2; RT-PCR: reverse transcription polymerase chain reaction; T-DXd: Trastuzumab deruxtecan; D: day; C: cycle; IF: Immunofluorescence; WES: whole exome sequencing; IHC: immunohistochemistry.

Extended Data Fig. 7 | Tissue and blood samples per time point and cohort used for translational analyses. Cohort 1: HER2-overexpressing (HER2 IHC 3+ or *ERBB2* ISH+) mBC, cohort 2: HER2-low (HER2 IHC 2+/*ERBB2* ISH- or IHC 1+) mBC, cohort 3: HER2 non-expressing (HER2 IHC 0) mBC.



Extended Data Fig. 8 | Immune cell density at 0 to 10 μm of tumor cells, in baseline and on treatment tumor biopsies in cohort 1 (HER2-overexpressing, $n = 18$). A significant decrease in tumor cell-proximate macrophage was observed during treatment (FDR-adjusted $p = 0.0305$). Blue bullets and red ones

represents at baseline and on-treatment samples, respectively. P -values were calculated using the Wilcoxon matched-pairs signed-rank test and adjusted for multiple hypothesis testing using the Benjamini-Hochberg method. All statistical tests were two sided.

Extended Data Table 1 | Number (%) of patients who developed adverse effects in the safety population

	Overall population n=179	Cohort 1 n=68	Cohort 2 n=73	Cohort 3 n=38
All grade AEs	179 (100%)	68 (100%)	73 (100%)	38 (100%)
Grade 3/4 AEs	88 (49.2%)	32 (47.1%)	40 (54.8%)	16 (42.1%)
Grade 5 AEs	3 (1.7%)	2 (2.9%)	-	1 (2.6%)
All grade TRAEs*	173 (96.6%)	67 (98.5%)	72 (98.6%)	34 (89.5%)
Grade 3/4 TRAEs	64 (35.8%)	23 (33.8%)	29 (39.7%)	12 (31.6%)
All grade SAEs	54 (30.2%)	23 (33.8%)	23 (31.5%)	8 (21.1%)
Treatment related SAEs	30 (16.8%)	12 (17.6%)	13 (17.8%)	5 (13.2%)

n: number of patients; AEs: adverse events; TRAEs: treatment-related adverse events; SAEs: serious adverse events.

*No TRAEs Grade 5 were observed.

Extended Data Table 2 | Number (%) of patients who experienced adverse effects and treatment-related adverse effects of grade > 2 in the safety population

SOC	MedDRA Preferred Term	AEs n (%)				TRAEs n (%)			
		Overall population n=179	Cohort 1 n=68	Cohort 2 n=73	Cohort 3 n=38	Overall population n=179	Cohort 1 n=68	Cohort 2 n=73	Cohort 3 n=38
Blood and lymphatic system disorders	Anaemia	9 (5.0%)	3 (4.4%)	4 (5.5%)	2 (5.3%)	7 (3.9%)	2 (2.9%)	4 (5.5%)	1 (2.6%) ¹
	Bone Marrow Failure	1 (0.6%)	-	1 (1.4%)	-	1 (0.6%)	-	1 (1.4%) ¹	-
	Neutropenia	21 (11.7%)	6 (8.8%)	12 (16.4%)	3 (7.9%)	21 (11.7%)	6 (8.8%) ¹	12 (16.4%)	3 (7.9%)
	Thrombocytopenia	1 (0.6%)	-	-	1 (2.6%)	1 (0.6%)	-	-	1 (2.6%)
Investigations	Alanine Aminotransferase Increased	2 (1.1%)	-	2 (2.7%)	-	1 (0.6%)	-	1 (1.4%)	-
	Aspartate Aminotransferase Increased	3 (1.7%)	1 (1.5%)	1 (1.4%)	1 (2.6%)	1 (0.6%)	1 (1.5%)	-	-
	Blood Alkaline Phosphatase Increased	3 (1.7%)	-	3 (4.1%)	-	-	-	-	-
	Blood Bilirubin Increased	1 (0.6%)	-	1 (1.4%)	-	-	-	-	-
	Blood Electrolytes Abnormal	1 (0.6%)	-	1 (1.4%)	-	-	-	-	-
	Ejection Fraction Decreased	1 (0.6%)	1 (1.5%)	-	-	1 (0.6%)	1 (1.5%)	-	-
	Electrocardiogram QT Prolonged	4 (2.2%)	4 (5.9%)	-	-	2 (1.1%)	2 (2.9%)	-	-
	Gamma-Glutamyltransferase Increased	10 (5.6%)	3 (4.4%)	7 (9.6%)	-	3 (1.7%)	2 (2.9%)	1 (1.4%)	-
	Lymphocyte Count Decreased	10 (5.6%)	6 (8.8%)	3 (4.1%)	1 (2.6%)	6 (3.4%)	4 (5.9%)	1 (1.4%)	1 (2.6%)
	Platelet Count Decreased	8 (4.5%)	3 (4.4%)	2 (2.7%)	3 (7.9%)	5 (2.8%)	1 (1.5%)	1 (1.4%) ¹	3 (7.9%) ²
	Weight Decreased	1 (0.6%)	-	1 (1.4%)	-	-	-	-	-
	White Blood Cell Count Decreased	8 (4.5%)	4 (5.9%)	3 (4.1%)	1 (2.6%)	8 (4.5%)	4 (5.9%) ¹	3 (4.1%)	1 (2.6%)
General disorders and administration site conditions	Fatigue	15 (8.4%)	6 (8.8%)	5 (6.8%)	4 (10.5%)	14 (7.8%)	6 (8.8%)	5 (6.8%)	3 (7.9%)
	General Physical Health Deterioration	1 (0.6%)	-	-	1 (2.6%) ¹	-	-	-	-
	Malaise	1 (0.6%)	1 (1.5%)	-	-	1 (0.6%)	1 (1.5%)	-	-
	Mucosal Inflammation	2 (1.1%)	-	2 (2.7%)	-	2 (1.1%)	-	2 (2.7%)	-
	Pain	1 (0.6%)	-	1 (1.4%)	-	-	-	-	-
	Pyrexia	1 (0.6%)	-	1 (1.4%)	-	-	-	-	-
Gastrointestinal disorders	Abdominal Pain	2 (1.1%)	-	2 (2.7%)	-	-	-	-	-
	Diarrhea	3 (1.7%)	-	3 (4.1%)	-	3 (1.7%)	-	3 (4.1%)	-
	Flatulence	1 (0.6%)	-	-	1 (2.6%)	1 (0.6%)	-	-	1 (2.6%)
	Intestinal Obstruction	2 (1.1%)	-	1 (1.4%)	1 (2.6%)	-	-	-	-
	Nausea	8 (4.5%)	1 (1.5%)	5 (6.8%)	2 (5.3%)	8 (4.5%)	1 (1.5%)	5 (6.8%)	2 (5.3%)
	Peritoneal Haemorrhage	3 (1.7%)	-	3 (4.1%)	-	-	-	-	-
	Subileus	1 (0.6%)	-	1 (1.4%)	-	-	-	-	-
	Vomiting	11 (6.1%)	2 (2.9%)	7 (9.6%)	2 (5.3%)	8 (4.5%)	1 (1.5%)	6 (8.2%)	1 (2.6%)
Metabolism and nutrition disorders	Decreased Appetite	2 (1.1%)	-	1 (1.4%)	1 (2.6%)	1 (0.6%)	-	-	1 (2.6%)
	Hyperalbuminaemia	1 (0.6%)	-	1 (1.4%)	-	-	-	-	-
	Hypercalcaemia	3 (1.7%)	-	2 (2.7%)	1 (2.6%)	1 (0.6%)	-	1 (1.4%)	-
	Hyperkalaemia	2 (1.1%)	2 (2.9%)	-	-	-	-	-	-
	Hypokalaemia	3 (1.7%)	1 (1.5%)	2 (2.7%)	-	1 (0.6%)	-	1 (1.4%)	-
	Hyponatremia	2 (1.1%)	-	2 (2.7%)	-	-	-	-	-
Respiratory, thoracic, and mediastinal disorders	Cough	1 (0.6%)	-	1 (1.4%)	-	1 (0.6%)	-	1 (1.4%)	-
	Dyspnea	2 (1.1%)	1 (1.5%)	1 (1.4%)	-	-	-	-	-
	Lung Disorder	1 (0.6%)	1 (1.5%) ³	-	-	-	-	-	-
	Pleural Effusion	1 (0.6%)	1 (1.5%)	-	-	-	-	-	-
	Pleuritic Pain	1 (0.6%)	-	1 (1.4%)	-	-	-	-	-
	Pneumothorax	1 (0.6%)	1 (1.5%)	-	-	-	-	-	-
	Pulmonary Embolism	2 (1.1%)	-	1 (1.4%)	1 (2.6%)	-	-	-	-
	Respiratory Distress	1 (0.6%)	-	-	1 (2.6%)	-	-	-	-
Infections and infestations	Device Related Sepsis	1 (0.6%)	-	1 (1.4%)	-	-	-	-	-
	Injection Site Infection	1 (0.6%)	-	1 (1.4%)	-	-	-	-	-
	Lung Infection	1 (0.6%)	1 (1.5%)	-	-	-	-	-	-
	Pneumocystis Jirovecii Pneumonia	1 (0.6%)	1 (1.5%)	-	-	1 (0.6%)	1 (1.5%)	-	-
	Pyelonephritis	1 (0.6%)	-	1 (1.4%)	-	-	-	-	-
	Rhinitis	1 (0.6%)	-	1 (1.4%)	-	1 (0.6%)	-	1 (1.4%)	-
	Sepsis	1 (0.6%)	-	1 (1.4%)	-	-	-	-	-
Musculoskeletal and connective tissue disorders	Back Pain	2 (1.1%)	1 (1.5%)	1 (1.4%)	-	-	-	-	-
	Pain In Extremity	1 (0.6%)	-	1 (1.4%)	-	-	-	-	-
	Pathological Fracture	1 (0.6%)	-	-	1 (2.6%)	-	-	-	-
	Spinal Pain	1 (0.6%)	1 (1.5%)	-	-	-	-	-	-
Skin and subcutaneous tissue disorders	Alopecia	3 (1.7%)	1 (1.5%)	1 (1.4%)	1 (2.6%)	3 (1.7%)	1 (1.5%)	1 (1.4%)	1 (2.6%)
	Skin Ulcer	1 (0.6%)	1 (1.5%)	-	-	-	-	-	-
Nervous system disorders	Brain Edema	2 (1.1%)	1 (1.5%) ³	1 (1.4%)	-	-	-	-	-
	Neuropathy Peripheral	1 (0.6%)	1 (1.5%)	-	-	1 (0.6%)	1 (1.5%)	-	-
Ear and labyrinth disorders	Deafness Unilateral	1 (0.6%)	-	-	1 (2.6%)	-	-	-	-
Cardiac disorders	Pericardial Effusion	1 (0.6%)	1 (1.5%)	-	-	1 (0.6%)	1 (1.5%) ¹	-	-
Psychiatric disorders	Anxiety	1 (0.6%)	-	1 (1.4%)	-	-	-	-	-
Renal and urinary disorders	Renal failure	1 (0.6%)	-	-	1 (2.6%)	1 (0.6%)	-	-	1 (2.6%)

n: number of patients; SOC: System Organ Class; MedDRA: Medical Dictionary for Regulatory Activities; AEs: adverse events; TRAEs: treatment-related adverse events

¹Including one patient with TRAEs grade 4²Including two patients with TRAEs grade 4³Including one patient with AEs grade 5

Reporting Summary

Nature Portfolio wishes to improve the reproducibility of the work that we publish. This form provides structure for consistency and transparency in reporting. For further information on Nature Portfolio policies, see our [Editorial Policies](#) and the [Editorial Policy Checklist](#).

Statistics

For all statistical analyses, confirm that the following items are present in the figure legend, table legend, main text, or Methods section.

n/a	Confirmed
<input type="checkbox"/>	<input checked="" type="checkbox"/> The exact sample size (<i>n</i>) for each experimental group/condition, given as a discrete number and unit of measurement
<input type="checkbox"/>	<input checked="" type="checkbox"/> A statement on whether measurements were taken from distinct samples or whether the same sample was measured repeatedly
<input type="checkbox"/>	<input checked="" type="checkbox"/> The statistical test(s) used AND whether they are one- or two-sided <i>Only common tests should be described solely by name; describe more complex techniques in the Methods section.</i>
<input type="checkbox"/>	<input checked="" type="checkbox"/> A description of all covariates tested
<input type="checkbox"/>	<input checked="" type="checkbox"/> A description of any assumptions or corrections, such as tests of normality and adjustment for multiple comparisons
<input type="checkbox"/>	<input type="checkbox"/> A full description of the statistical parameters including central tendency (e.g. means) or other basic estimates (e.g. regression coefficient) AND variation (e.g. standard deviation) or associated estimates of uncertainty (e.g. confidence intervals)
<input type="checkbox"/>	<input checked="" type="checkbox"/> For null hypothesis testing, the test statistic (e.g. <i>F</i> , <i>t</i> , <i>r</i>) with confidence intervals, effect sizes, degrees of freedom and <i>P</i> value noted <i>Give P values as exact values whenever suitable.</i>
<input checked="" type="checkbox"/>	<input type="checkbox"/> For Bayesian analysis, information on the choice of priors and Markov chain Monte Carlo settings
<input checked="" type="checkbox"/>	<input type="checkbox"/> For hierarchical and complex designs, identification of the appropriate level for tests and full reporting of outcomes
<input type="checkbox"/>	<input checked="" type="checkbox"/> Estimates of effect sizes (e.g. Cohen's <i>d</i> , Pearson's <i>r</i>), indicating how they were calculated

Our web collection on [statistics for biologists](#) contains articles on many of the points above.

Software and code

Policy information about [availability of computer code](#)

Data collection	Patients and samples attributes for the TCGA breast cancer study were downloaded from the GDC data portal using the R package GenomicDataCommons version 1.18.0. Data collection was performed with CSONline modul from Ennov Clinical.
Data analysis	WES alignment: Raw sequence data were aligned to the human genome (NCBI build 37) using BWA version 0.7.17. Base qualities were recalibrated using BaseRecalibrator and ApplyBQSR tools from GATK bundle v4.1.8.1. WES quality-control: Raw sequence data quality was controlled using FastQC v0.11.8. Sequencing reads were processed by fastp v0.20 prior to alignment. Alignment quality was controlled using SAMtools v1.9, and GATK v4.1.8.1. SNVs and indels were called using Mutect2 from GATK v4.1.8.1. CNAs were identified using FACETS R package v0.5.14. SNVs and indels were filtered using GATK v4.1.8.1 filtering procedure from the best practices. For MIF analysis, the WSI were analyzed with QuPath 0.3.2. Analysis of the slides stained for HER2 expression were performed using Python version 3.9, Openslide version 3.4.1, Pytorch version 1.9.0, and Scikit-Learn version 0.24.2. Nuclei features were computed on QuPath version 0.4.0. The source to reproduce the analyses supporting the analyses presented in the paper is available at https://github.com/gustaveroussy/DAISY_Public . Statistical analyses were carried out using Stata software v16 (StataCorp, Texas, US). For in vitro experiments, statistical analysis was performed using GraphPad Prism 9 (GraphPad Software).

For manuscripts utilizing custom algorithms or software that are central to the research but not yet described in published literature, software must be made available to editors and reviewers. We strongly encourage code deposition in a community repository (e.g. GitHub). See the Nature Portfolio [guidelines for submitting code & software](#) for further information.

Data

Policy information about [availability of data](#)

All manuscripts must include a [data availability statement](#). This statement should provide the following information, where applicable:

- Accession codes, unique identifiers, or web links for publicly available datasets
- A description of any restrictions on data availability
- For clinical datasets or third party data, please ensure that the statement adheres to our [policy](#)

All data used in the present study are available within the manuscript and its supplementary information files.

Clinical data is available for access upon external requests. Applicants should contact the following email address “mariafernanda.mosele@gustaveroussy.fr” to request access to clinical data. The request will be discussed internally in the joint steering committee of the study. The decision will be communicate within one month from the request. Applicants must complete specific documents in order to be granted a user license.

WES data generated in this study have been deposited to the European Genome-Phenome Archive (EGA) under the accession number EGAD00001011110. Please refer to the forms and README file from

https://github.com/gustaveroussy/DAISY_Public/tree/master/data

for instructions on how to access the data. Other data that support the findings of this study are available from the corresponding author upon request.

SNVs and indels for TCGA breast cancer samples were downloaded with permission from the file mc3.v.0.2.8.CONTROLLED.maf.gz (<https://gdc.cancer.gov/about-data/publications/mc3-2017>). Raw WES data of TCGA breast cancer samples were downloaded with permission from the GDC-controlled Google Cloud bucket [gs://gdc-tcga-phs000178-controlled](https://gdc-tcga-phs000178-controlled).

Databases used in the study include gnomAD (<https://gnomad.broadinstitute.org>), OncoKB Precision Oncology Knowledge Base (<https://www.oncokb.org>), Clinical Interpretation of Variants in Cancer (<https://civicedb.org>), dbNSFP version 4.1.a (<https://sites.google.com/site/jpopgen/dbNSFP>).

Research involving human participants, their data, or biological material

Policy information about studies with [human participants or human data](#). See also policy information about [sex, gender \(identity/presentation\), and sexual orientation](#) and [race, ethnicity and racism](#).

Reporting on sex and gender

Findings from DAISY trial apply to both sexes. Sex was determined based on self-reporting. Gender was not considered in study design.

Reporting on race, ethnicity, or other socially relevant groupings

Race or ethnicity analyses was not performed in DAISY trial since it is forbidden in France.

Population characteristics

Patients presented metastatic breast cancer with any hormone receptor and HER2 status. For cancers, with expression of hormone receptors, the patients were included if they presented resistance to endocrine therapy and CDK4/6 inhibitors. For patients with HER2-overexpressing breast cancer they must have progressed on Trastuzumab and TDM1. Patients must have received at least one line of chemotherapy in the metastatic setting. Patients must have received at least one line of chemotherapy in the metastatic setting. In the DAISY trial, 186 patients were enrolled and 179 were included in the safety population. The median age of the population is 55 years. 99.4% of the patientes are women and 0.6% men. At baseline, 43% of patients presented a PSO and 71.5% presented hormone receptor positive breast cancer. 64.8% of patients presented 3 or more metastatic sites at baseline and 57.6% of patients presented liver metastasis. 53% of patients received 5 or more lines of previous therapies in the metastatic setting. The median interval from initial diagnosis to metastatic disease was 25.8 months and the median interval from metastatic diagnosis to inclusion was 43.7 months.

Recruitment

186 patients meeting the clinical trial eligibility criteria were recruited during clinical consultation with oncologists. The first patient was enrolled on November 4th 2019 and the last one on March 3rd 2021 in 15 study centers in France. We did not identify self-selection bias or other bias that could impact the results.

Ethics oversight

All patients who entered in DAISY trial signed an informed consent. DAISY trial was approved by the French ethics committee, CPP – Ile de France on September 05th 2019 and the French health authorities, ANSM, on July 08th 2019.

Note that full information on the approval of the study protocol must also be provided in the manuscript.

Field-specific reporting

Please select the one below that is the best fit for your research. If you are not sure, read the appropriate sections before making your selection.

☒ Life sciences ☐ Behavioural & social sciences ☐ Ecological, evolutionary & environmental sciences

For a reference copy of the document with all sections, see nature.com/documents/nr-reporting-summary-flat.pdf

Life sciences study design

All studies must disclose on these points even when the disclosure is negative.

Sample size	The primary endpoint was the confirmed objective response rate evaluated in each cohort, defined as the presence of a confirmed partial or complete response assessed by investigators. The investigator evaluated the objective response using RECIST v1.1 criteria. The required number of assessable patients for cohort 1 (n=67) and 2 (n=40) was determined using the A'Hern design with the following hypothesis: Cohort 1 (p0 = 30%; p1 = 45%, alpha = 5%, 1-beta = 80%) and Cohort 2 (p0 = 20%; p1 = 40%, alpha = 5%, power= 85%). The regimen would be declared promising in cohort 1 if 27 patients present a confirmed objective response among 67 and in cohort 2 if 13 confirmed objective response were observed among 40. Cohort 3 was designed using an optimal two stage design (alpha = 5%, power= 85%) with non-progression at 3 months as short-term endpoint (p20=30% and p21=50%) and confirmed objective response as primary endpoint (p10=20%, p11=40%). A stop for non-promising activity was planned to be declared if 4 patients or less among the first 16 present non-progressive disease at 3 months. At final analysis of cohort 3, the regimen would be defined as promising if 13 patients or more present a confirmed objective response among 40. In cohort 3, recruitment was stopped after 40 patients (37 assessable for activity) because slow recruitment. For each cohort, it was assume a rate of 10% non-evaluable patients and sample size was increased: Cohort 1: n=74, Cohort 2: n=44, Cohort 3: n=44. Full details are provided in statistical analysis plan.
Data exclusions	Of the 186 patients included in DAISY trial, 7 patients who did not receive at least one dose of T-DXd were excluded from the safety population and 2 additional patients who did not have a valid first post-baseline assessment of disease status or who did not have progressive disease were excluded from the Full Analysis Set population as planned in the statistical analysis plan. Annex 3 includes all analyses that have been done by the statistician. For HER2 spatial sitribution analyses, 7 patients (cohort 1) and 7 patients (cohort 2) were excluded because HER2 slides were not exploitable or could not be digitalized with the appropriate scanner. For T-Dxd distribution on-treatment, 3 out of 10 pairs of biopsies were not analyzable because of absence of cancer cells. For the RT-PCR tumor samples with <30% of tumor cells were excluded. For WES analyses, tumor samples with <30% of tumor cells were excluded.
Replication	Since the paper reports a prospective clinical trial, there is no attempt to replicate the finding in the same paper. Nevertheless, the primary objective of the study was predefined and thus limits the risk of non replication.
Randomization	The trial was a phase II ,single arm, not randomized trial. Patients were allocated into the different cohorts according to HER2 level expression.
Blinding	Investigators were not blinded regarding cohort assignment. Blinding was not considered relevant since the oncologist knew the HER2 status of the patient.

Reporting for specific materials, systems and methods

We require information from authors about some types of materials, experimental systems and methods used in many studies. Here, indicate whether each material, system or method listed is relevant to your study. If you are not sure if a list item applies to your research, read the appropriate section before selecting a response.

Materials & experimental systems

Methods

n/a	Involved in the study	n/a	Involved in the study
<input type="checkbox"/>	<input checked="" type="checkbox"/> Antibodies	<input checked="" type="checkbox"/>	<input type="checkbox"/> ChIP-seq
<input type="checkbox"/>	<input checked="" type="checkbox"/> Eukaryotic cell lines	<input checked="" type="checkbox"/>	<input type="checkbox"/> Flow cytometry
<input checked="" type="checkbox"/>	<input type="checkbox"/> Palaeontology and archaeology	<input checked="" type="checkbox"/>	<input type="checkbox"/> MRI-based neuroimaging
<input checked="" type="checkbox"/>	<input type="checkbox"/> Animals and other organisms		
<input type="checkbox"/>	<input checked="" type="checkbox"/> Clinical data		
<input checked="" type="checkbox"/>	<input type="checkbox"/> Dual use research of concern		
<input checked="" type="checkbox"/>	<input type="checkbox"/> Plants		

Antibodies

Antibodies used	The antibody used for HER2 staining was a rabbit monoclonal primary antibody supplied by Roche, clone 4B5, reference 05999570001, pre-diluted ready to use. For the enhanced HER2 protocol, OptiView DAB IHC Detection Kit (Roche Diagnostics) was used instead of ultraView Universal DAB Detection Kit (Roche Diagnostics). Staining for DXd-IgG was performed using a primary antibody against DXd (antiXAFG5737-1A3-ocChimera, Daiichi Sankyo) with Leica BOND RX automated slide stainer (Leica Biosystems). Rabbit isotype control antibody (#PA0777, Leica Biosystems) was used as negative reagent control. MIF was performed with the ULTIVUE kit, reference ULT30801, containing the Immuno8 FixVUE panel containing eight pre-diluted antibodies according to manufacturer instructions ready to use. The panel of antibodies included: anti CD3 (clone BC33), anti CD4 (clone SP35), anti CD8 (clone C8/144B), anti CD68 (clone KP-1), anti FoxP3 (clone 236A/E7), anti PD-1 (clone CAL20), anti PD-L1 (clone 73-10), anti PanCK/SOX10 (clone AE1/AE3/BC34).
Validation	Each primary antibody is tested and optimized for ISP and has as reference the corresponding DAB. Expert pathologist assess quality of ISP staining (eg sensitivity, specificity, staining pattern, signal/background ratio) in multiple indications including tissue positive

controls and tumor types as compared to serial sections stained with classical DAB IHC. Primary antibodies developed for ISP are already validated for FFPE applications.

Immuno8 FixVUE panel has also been validated as a panel by performing precision testing and reproducibility in several studies. You can refer to our website for the Immuno8 FixVUE panel validation.

The specificity of the anti-DXd antibody was confirmed by the fact that DXd staining disappeared in IHC when the antibody was preincubated with DXd, while it did not disappear when preincubated with SN-38. For more information refer to <https://doi.org/10.1158/1078-0432.CCR-21-0397>.

Eukaryotic cell lines

Policy information about [cell lines and Sex and Gender in Research](#)

Cell line source(s)	MCF-7 and SK-BR-3 cells were purchased from DSMZ (Germany). These cell lines are derived from two female patients respectively with breast cancer.
Authentication	None of these cell lines were authenticated.
Mycoplasma contamination	The cell lines were not tested for mycoplasma contamination.
Commonly misidentified lines (See ICLAC register)	The cell lines used in the study are cell lines commonly used.

Clinical data

Policy information about [clinical studies](#)

All manuscripts should comply with the ICMJE [guidelines for publication of clinical research](#) and a completed [CONSORT checklist](#) must be included with all submissions.

Clinical trial registration	NCT04132960
Study protocol	Annexes 1 and 2 were submitted with the first submission of the DAISY trial
Data collection	The trial included patients from November 2019 to March 2021. Data were captured by clinical research assistants in the centers that participated to the trial using a eCRF. Data was collected with CSONline from Ennov Clinical. Trial monitoring was done on a regular basis by the sponsor UNICANCER.
Outcomes	<p>The primary endpoint was the confirmed objective response rate evaluated in each cohort, defined as the presence of a confirmed partial or complete response assessed by investigators. The investigator evaluated the objective response using RECIST v1.1 criteria. For the cohort 3 (IHC0+), a short term primary endpoint is used for the interim analysis. The short term primary endpoint was the rate of patient without progression at 3 months. The investigator evaluated the progression using RECIST v1.1.</p> <p>The secondary endpoints were predefined by the study steering committee. The secondary endpoints included progression-free survival (PFS), duration of response (DOR), overall survival (OS), and clinical benefit rate (CBR) and were evaluated on the Full Analysis Set (FAS) and per cohort.</p> <p>PFS was defined as the time from inclusion until progression or death from any cause. At the time of analysis, patients alive and without progression were censored at the date of the last tumor assessment. The investigator evaluated progression using RECIST v1.1.</p> <p>DOR was applicable to subject with objective response, either complete response (CR) or partial response (PR), and was defined as the time from the first documented CR or PR until progression or death from any cause. The objective response and progression were evaluated by investigator using RECIST v1.1.</p> <p>OS was defined as the time from inclusion to death from any cause. Patients still alive at the time of analysis were censored at the date of last follow up.</p> <p>CBR was defined as the presence of at least a CR or PR or stable disease > 6 months assessed by investigators using RECIST v1.1. More details are available in the statistical analysis plan.</p>